Int. J. Cancer: **112,** 365–375 (2004)

Publication of the International Union Against Cancer

LOW EXPRESSION OF HUMAN TUBULIN TYROSINE LIGASE AND SUPPRESSED TUBULIN TYROSINATION/DETYROSINATION CYCLE ARE ASSOCIATED WITH IMPAIRED NEURONAL DIFFERENTIATION IN NEUROBLASTOMAS WITH POOR PROGNOSIS

Chiaki KATO[1,2], Kou MIYAZAKI[1], Atsuko NAKAGAWA[3], Miki OHIRA[1], Yohko NAKAMURA[1], Toshinori OZAKI[1], Toshio IMAI[2] and Akira NAKAGAWARA[1]*

[1]*Division of Biochemistry, Chiba Cancer Center Research Institute, Chiba, Japan*
[2]*Department of Physiologic Chemistry Faculty of Science, Toho University, Chiba, Japan*
[3]*Second Department of Pathology, Aichi Medical University, Nagakute, Japan*

Neuroblastoma (NBL), one of the most common childhood solid tumors, has a distinct nature in different prognostic subgroups. However, the precise mechanism underlying this phenomenon remains largely unknown. To understand the molecular and genetic bases of neuroblastoma, we have generated its cDNA libraries and identified a human ortholog of *tubulin tyrosine ligase* gene (*hTTL/Nbla0660*) as a differentially expressed gene at high levels in a favorable subset of the tumor. Tubulin is subjected to several types of evolutionarily conserved posttranslational modification, including tyrosination and detyrosination. Tubulin tyrosine ligase catalyzes ligation of the tyrosine residue to the COOH terminus of the detyrosinated form of α-tubulin. The measurement of *hTTL* mRNA expression in 74 primary neuroblastomas by quantitative real-time reverse transcription-PCR revealed that its high expression was significantly associated with favorable stages (1, 2 and 4s; $p = 0.0069$), high *TrkA* expression ($p = 0.002$), a single copy of *MYCN* ($p < 0.00005$), tumors found by mass screening ($p = 0.0042$), nonadrenal origin ($p = 0.0042$) and good prognosis ($p = 0.023$). The log-rank test showed that high expression of *hTTL* was an indicator of favorable prognosis ($p = 0.026$). Immunohistochemical analysis using specific antibodies generated by us demonstrated that tyrosinated tubulin (Tyr-tubulin), detyrosinated tubulin (Glu-tubulin) and hTTL as well as Δ2-tubulin were positive in favorable tumors, whereas only Δ2-tubulin was positive in the tumors with *MYCN* amplification. In an RTBM1 neuroblastoma cell line, hTTL was increased after treating the cells with bone morphogenetic protein 2 (BMP2) or all-trans retinoic acid (RA), which induced neuronal differentiation. These results suggest that the deregulated tubulin tyrosination/detyrosination cycle caused by decreased expression of hTTL is associated with inhibition of neuronal differentiation and enhancement of cell growth in the primary neuroblastomas with poor outcome.

Key words: *tubulin tyrosine ligase; tubulin tyrosination; neuroblastoma; neuronal differentiation; prognostic factor*

Tubulin is one of the most important molecular components that regulate cytoskeletal structure relating to cell motility, cell division, differentiation, invasion and metastasis in cancer. However, functional modification of tubulin protein has still been elusive. Tubulin is subjected to several types of evolutionarily conserved posttranslational modification that includes tyrosination/detyrosination, acetylation, phosophorylation, palmitoylation, polyglutamylation and polyglycylation.[1–4] The discovery of tyrosination cycle stems from the serial observations that the addition of radiolabeled tyrosine to a rat brain cytosolic extract leads to tyrosination of the COOH terminus of a single endogenous protein, α-tubulin, by a translation-independent mechanism.[5–7] Posttranslational incorporation of tyrosine into the tubulin has also been shown to occur *in vivo*.[8–10] The cycle of tyrosination/detyrosination is evolutionarily conserved[11–13] and is regulated by both tubulin tyrosine ligase (TTL) and carboxypeptidase, the gene of which has not yet been identified (Fig. 1). Microtubule dynamics is also an important factor. TTL protein was first purified by immunoaffinity chromatography from the lysates of bovine and porcine brains and was extensively characterized by protein sequencing.[14] Recently, rat *TTL* cDNA has also been isolated.[15] Interestingly, in 1991, Paturle-Lafanechere *et al.*[16] identified a nontyrosinatable variant of tubulin that lacked 2 amino acid residues, glutamic acid and tyrosine, at the COOH terminus (Δ2-tubulin). Δ2-tubulin was found to accumulate in mature neurons and in stable microtubule assemblies in cells.[17,18] In some tumors, it also accumulated in the cellular cytoplasm in association with decreased levels of TTL, suggesting that the amount of Δ2-tubulin and TTL expression level in tumor cells are important to define the malignant grade of cancer.[19] However, pathophysiologic significance of the tyrosination/detyrosination cycle in normal and cancer cells still remains unclear.

Neuroblastoma (NBL) is one of the most common childhood solid tumors and has distinct biologic characteristics in different prognostic subgroups. For example, NBL in patients under 1 year of age usually regresses spontaneously, whereas that in patients over 1 year of age often grows aggressively and eventually kills the patient. To understand the molecular mechanism of distinct biology and tumorigenesis of NBL, we have previously performed a comprehensive approach to unveil the gene expression profiles among the NBL subsets.[20,21] We constructed the subset-specific oligo-capping cDNA libraries from the primary NBL tissues with favorable (stage 1, high expression of *TrkA* and a single copy of *MYCN*) and unfavorable (stage 3 or 4, decreased expression of *TrkA* and *MYCN* amplification) characteristics and randomly cloned 4,654 cDNAs. After adding the cDNAs obtained from the stage 4s NBL cDNA library to our NBL gene collection, we made an in-house cDNA microarray carrying 5,340 genes proper to NBL. The comprehensive analysis of 136 NBLs using the microar-

Abbreviations: BMP2, bone morphogenetic protein 2; DMEM, Dulbecco's modified Eagle's medium; ECL, enhanced chemiluminescence; FBS, fetal bovine serum; hTTL, human tubulin tyrosine ligase; NBL, neuroblastoma; RA, retinoic acid; TCP, tubulin carboxypeptidase; TTL, tubulin tyrosine ligase.

Grant sponsor: Grant-in-Aid for Scientific Research and for Scientific Research on Priority Areas, Medical Genome Science from the Ministry of Education, Science, Sports and Culture, Japan; Grant sponsor: Hisamitsu Pharmaceutical Co. Inc.

*Correspondence to: Division of Biochemistry, Chiba Cancer Center Research Institute, 666-2 Nitona, Chuoh-ku, Chiba 260-8717, Japan. Fax: +81-43-265-4459. E-mail: akiranak@chiba-ccri.chuo.chiba.jp

Received 27 January 2004; Accepted 15 April 2004

DOI 10.1002/ijc.20431
Published online 23 June 2004 in Wiley InterScience (www.interscience.wiley.com).

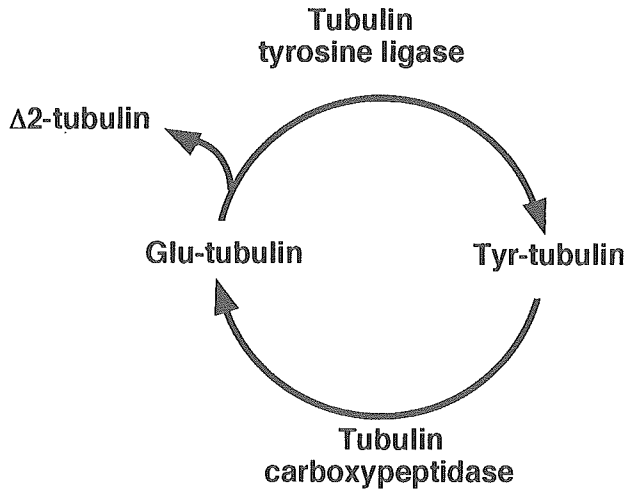

FIGURE 1 – The tyrosination/detyrosination cycle catalyzed by tubulin tyrosine ligase and tubulin carboxypeptidase.

ray showed that many genes that are related to the cytoskeletal components, including α-tubulin, had prognostic significance (data not shown).

In the present study, we have cloned for the first time the human ortholog of TTL (*hTTL*) from both the NBL and a fetal brain cDNA libraries. The analysis using 74 primary NBLs shows that expression of *hTTL* mRNA is significantly lower in unfavorable NBLs than in favorable tumors. The examination using specific antibodies raised against hTTL, Tyr-tubulin, Glu-tubulin and Δ2-tubulin demonstrates that hTTL is increased during induction of neuronal differentiation of cultured NBL cells treated with BMP2 or RA. The immunohistochemical study shows that hTTL, Tyr-tubulin, Glu-tubulin and Δ2-tubulin are positive in favorable NBLs, whereas only Δ2-tubulin is positive in aggressive NBLs with *MYCN* amplification. These suggested that the tyrosination/detyrosination cycle of α-tubulin is active in NBLs with high potential to differentiate or undergo apoptosis, while it is disregulated by downregulation of hTTL in *MYCN*-amplified NBLs, resulting in accumulation of Δ2-tubulin.

MATERIAL AND METHODS

Tumor specimen

Fresh frozen tumor tissues obtained by surgery or biopsy were sent to the Division of Biochemistry, Chiba Cancer Center Research Institute, from various hospitals in Japan with informed consent. Ninety tumors examined in this study were staged according to the International Neuroblastoma Staging System (INSS).[22] The number of tumors subjected to quantitative real-time RT-PCR were 24 in stage 1, 11 in stage 2, 5 in stage 4s, 10 in stage 3 and 24 in stage 4. The patients were treated according to the protocols previously described.[23] Biologic information on each tumor, including *MYCN* gene copy number, *TrkA* gene expression and DNA ploidy, was analyzed in our laboratory as described previously.[24]

Cell culture and transfection

COS7 and HEK293T cells were maintained in Dulbecco's modified Eagle's medium (DMEM) supplemented with 10% heat-inactivated fetal bovine serum (FBS; Life Technologies, Gaithersburg, MD) and penicillin (100 IU/ml)/streptomycin (100 μg/ml). Human neuroblastoma RTBM1 cells were grown in RPMI-1640 medium containing 10% heat-inactivated FBS and antibiotic mixture. Cultures were maintained at 37°C in a water-saturated atmosphere of 5% CO_2 in air. Transient transfection was performed by LipofectAMINE 2000 transfection reagent (Invitrogen, Carlsbad, CA) according to the manufacturer's instructions. In brief, cells were seeded in tissue culture plates to achieve 50% confluence. Twenty-four hours later, cells were transfected by using a mixture of the expression plasmids and LipofectAMINE 2000 transfection reagent in DMEM without serum. Forty-eight hours after transfection, cells were collected and analyzed by Western blotting. For neurite extension assays, RTBM1 cells were treated either with recombinant human BMP2 (Yamanouchi Pharmaceutical, Tokyo, Japan) or with RA at a final concentration of 1 nM or 5 μM, respectively.

RNA isolation and semiquantitative RT-PCR

Total RNA was prepared from neuroblastoma tissues according to the AGPC method.[25] Five micrograms of total RNA were subjected to the synthesis of the first-strand cDNA with pd$(N)_6$ random hexamer (Takara Shuzo, Otsu, Japan) and a Superscript II reverse transcriptase (Invitrogen) at 42°C for 90 min. The resultant cDNA was diluted to be a 1:20 solution and was amplified in a final volume of 10 μl of reaction mixture containing 100 μM of each deoxynucleoside triphosphate, 1 × PCR buffer, 1 μM of each primer and 0.2 U of rTaq DNA polymerase (Takara Bio, Ohtsu, Japan). The following primers were used: *hTTL*, 5′-CAGCTCTTCGGCTTTGACTT-3′ (sense) and 5′-GCTGTGGGCTGGATAAAGAG-3′ (antisense); human *GAPDH*, 5′-ACCTGACCTGCCGTCTAGAA-3′ (sense) and 5′-TCC ACCACCCTGTTGCTGTA-3′ (antisense). PCR templates were standardized by its *GAPDH* expression before performing semiquantitative PCR experiment. The PCR-amplified products were separated by electrophoresis on a 1.5% agarose gel and visualized by ethidium bromide poststaining.

Quantitative real-time RT-PCR

cDNA was prepared by the same method as in the semiquantitative RT-PCR and 2 μl of the 40-fold dilution was used for each PCR reaction. Primers and TaqMan probes for *hTTL* were designed using the primer design software Primer Express (Perkin-Elmer Applied Biosystems, Foster City, CA). The primer sequences for *hTTL* are 5′-AAGGAACTGCCTCCTGAGC-3′ and 5′-TCAATGAGCCAC ACCTTCA-3′. The probe sequence for *TTL* is 5′-FAM-ATTAGC ACCAAGCACCTCCCTTACCAGAGC-TAMRA-3′. PCR was carried out with the ABI Prism 7700 Sequence Detection System (Perkin-Elmer Applied Biosystems). Two μl of cDNA was amplified in a final volume of 25 μl containing 1 × TaqMan mixture, 300 nM each primer and 200 nM TaqMan probe. The thermal cycling condition was as follows: 50 cycles of a 2-step PCR (95°C for 15 sec, 60°C for 1 min) after the initial activation of UNG followed by denaturation (50°C for 2 min, 95°C for 10 min). TaqMan *GAPDH* control reagent kit (Roche Molecular Biochemicals, Basel, Switzerland) was used for the amplification of *GAPDH* according to the manufacturer's instructions; all data were normalized using *GAPDH* expression. The experiments were performed in triplicate for each data point.

Generation of polyclonal anti-hTTL antibodies

The polyclonal anti-hTTL antibody was raised in rabbits against Cys-coupled synthetic peptides derived from hTTL (222-RTASEPY-HVDNFQDKTCHLTNH-243 and 244-CIQKEYSKNYGKYEE-GNE-261). The polyclonal anti-Tyr-tubulin, anti-Glu-tubulin and anti-Δ2-tubulin antibodies were raised in rabbits immunized with Cys-coupled synthetic peptides corresponding to their COOH termini (CEEEGEEY, CGEEEGEE and CEGEEEGE, respectively). Antibodies were purified by using peptide-coupled affinity columns and tested for their ability to identify the corresponding proteins by Western blots. The synthetic peptides and antibodies were generated by Protein Express (Chiba, Japan).

Construction of FLAG-tagged hTTL expression plasmid

The FLAG-tagged hTTL expression plasmid was generated by PCR amplification using the cDNA library derived from human fetal brain (Stratagene, La Jolla, CA) and an *hTTL* cDNA that lacked the 5′-portion encoding the NH_2 terminal region of hTTL as templates. The forward and reverse primers used were 5′-TAAATAGTCGACGATATCATGGACTACAAGGACGAC

GACGACAAGTACACCTTCGTGGTACGCGATGAGAACAGC AGCGTCTACGCCGAGGTCTCCCGGCTGCTCCTCGCCA-3′ (sequence encoding FLAG epitope tag is in boldface, and *Eco*RV recognition site is underlined) and 5′-TACATGTCGACGCGG CCGCTCACAGCTTGAT GAA-3′ (*Not*I restriction site is underlined). The resulting PCR product was gel-purified, digested with *Eco*RV and *Not*I, inserted into identical restriction sites of a mammalian expression plasmid pIRESpuro2 (Clontech Laboratories, Palo Alto, CA) and its nucleotide sequence was verified by automated dideoxy terminator cycle sequencing.

Western blot analysis

Cells were washed in ice-cold phosphate-buffered saline (PBS), collected by centrifugation and lysed in 1 × sample buffer. Equal amounts of whole-cell lysates were fractionated by SDS-polyacrylamide gel electrophoresis (SDS-PAGE), and electrophoretically transferred onto a polyvinylidene difluoride (PVDF) membrane filter (Immobilon-P; Millipore, Billerica, MA). The filter was then blocked with Tris-buffered saline (TBS) containing 5% nonfat dry milk at room temperature for 1 hr and subsequently incubated for 1 hr with the antibodies against hTTL, Tyr-tubulin, Glu-tubulin, Δ2-tubulin, α-tubulin (5H1; PharMingen, San Diego, CA) and actin (20-33; Sigma Chemical, St. Louis, MO). The filter was further incubated with horseradish peroxidase-conjugated mouse or rabbit IgG secondary antibody (Cell Signaling Technologies, Beverly, MA). Immunoreactivity was detected using the enhanced chemiluminescence system (ECL; Amersham Pharmacia Biotechnology, Uppsala, Sweden) according to the manufacturer's instructions. The films were exposed at multiple time points to ensure that the images were not saturated.

Immunohistochemistry

Immunohistochemical stainings with antibodies against hTTL (1:100), Tyr-tubulin (1:100), Glu-tubulin (1:100) and Δ2-tubulin (1:100) were performed on 10 human neuroblastoma tumors selected from the surgical pathology file at the Department of Pathology, Aichi Medical University, based on the results of histopathology evaluation[26] and *MYCN* status. Also performed were immunostainings with antibodies against TrkA (1:40, 763; Santa Cruz Biotechnology, Santa Cruz, CA), CD56 (1B6; Novocastra Laboratories, Peterborough, U.K.) and Ki-67 (1:200, MIB-1; Dako, Kyoto, Japan) on the same tumor tissues. All of those tumor samples were obtained prior to chemotherapy and irradiation therapy and included 6 favorable histology cases with nonamplified *MYCN* (FH&NA) and 4 unfavorable histology cases with amplified *MYCN* (UH&A). Among the neuroblastoma cases, tumors in the FH&NA subset were reported to be the most favorable biologically and clinically. In contrast, tumors in the UH&A subset are known to be the most aggressive with the poorest clinical outcome.[27] Four μm thick sections from the formalin-fixed and paraffin-embedded tissue samples were deparaffinized and microwaved for 3 × 5 min in Na-citrate buffer (pH 6.0) for antigen retrieval. The slides were first immersed in 0.3% hydrogen peroxide in methanol for 20 min and then in 10% normal goat serum for 30 min. The primary antibodies were then applied at 4°C overnight, followed by a standard staining procedure using the Vectastain ABC kit (Vector Laboratories, Burlingame, CA). Sections were counterstained with hematoxylin for light microscopic review and evaluation. hTTL, Tyr-tubulin, Glu-tubulin and Δ2-tubulin were always positively detected in the cytoplasm and neuritic processes of normal ganglion cells in the separate positive control sections as well as in the test sections as built-in control, whenever available. As for the negative controls of hTTL, Tyr-tubulin, Glu-tubulin, Δ2-tubulin and TrkA stainings, normal rabbit immunoglobulins (1:500 dilution, Vector Laboratories) were applied as the primary antibody. As for the negative controls of CD56 and Ki-67 stainings, we followed the staining procedure without the primary antibodies.

Statistical analysis

Student's *t*-tests were used to explore possible associations between *hTTL* expression and other factors, such as age. Since the values of the *hTTL* expression were skewed, a log transformation was used to achieve the normality when using *t*-test and Cox regression. The distinction between high and low levels of *hTTL* was based on the median value (low, *hTTL* < 95 e.u.; high, *hTTL* > 95 e.u.), regardless of tumor stage, *MYCN* copy number, or survival. Kaplan-Meier survival curves were calculated, and survival distributions were compared using the log-rank test. Cox regression models were used to explore associations between *hTTL* expression, age, *MYCN* amplification, mass screening, origin and survival. Statistical significance was declared if the *p*-value was < 0.05. Statistical analysis was performed using Stata 7.0. (Stata, College Station, TX).

RESULTS

Cloning and expression of hTTL *gene*

We have previously constructed oligo-capping cDNA libraries from 3 fresh human NBL tissues (stages 1 and 2, high *TrkA* expression and a single copy of *MYCN*), which were gradually undergoing spontaneous regression probably due to neuronal apoptosis.[20] Screening of 1,152 novel genes by reverse transcriptase (RT)-PCR revealed that 194 genes were expressed differentially between NBLs with favorable prognosis and those with unfavorable outcome. Among them, we detected a partial cDNA sequence (*Nbla00660*) corresponding to the human ortholog of *tubulin tyrosine ligase* (*hTTL*) gene. We then cloned the full-length *hTTL* cDNA using both conventional phage library screening and genome sequence-based RT-PCR procedure. The *hTTL* gene was mapped to chromosome 2q13 and consisted of 7 exons (Fig. 2*a*) with 377 predicted amino acids (Genbank/DDBJ accession number AB071393; Fig. 2*b*). Comparison of the deduced amino acid sequence of human *TTL* cDNA with those of mouse, rat, pig and cow showed identity by 94%, 94%, 93% and 94%, respectively. *hTTL* was ubiquitously expressed in various human tissues including heart, kidney, lung, colon, thymus, spleen, mammary gland, testis, prostate, brain, cerebellum, liver, fetal brain, fetal liver, adrenal gland and skeletal muscle (Fig. 2*c*). However, it was rather preferentially expressed in adult and fetal brains and lung.

Specific antibodies and catalytic activity of hTTL

To study the role of hTTL and the tyrosination/detyrosination cycle regulated by TTL in neuroblastoma, we generated specific antibodies against human Tyr-tubulin, Glu-tubulin and Δ2-tubulin based on the previous reports.[16,18,28] The PVDF membranes spotted with equal amount (1 μg) of synthetic peptides corresponding to COOH terminal 7 amino acid residues of Tyr-tubulin (CEEEGEEY), Glu-tubulin (CGEEEGEE) and Δ2-tubulin (CEGEEEGE) were immunoblotted with rabbit anti-Tyr-tubulin antibody (Fig. 3*a*, top), anti-Glu-tubulin antibody (Fig. 3*a*, middle) and anti-Δ2-tubulin antibody (Fig. 3*a*, bottom), respectively. There were no crossreactivities among them, suggesting that those 3 antibodies were highly specific to each form of tubulin. To confirm the catalytic activity of hTTL encoded by the gene we cloned, we transfected the HEK293T cells with various amount of *hTTL* expression construct. Increased levels of hTTL in those cells induced tyrosination of tubulin in dose-dependent manner, while the level of endogenous Glu-tubulin was decreased (Fig. 3*c*). These results showed that hTTL protein encoded by the gene we cloned has its catalytic activity.

Upregulation of hTTL expression during neuronal differentiation

BMP2 has been characterized as a neurotrophic factor.[29] Recently, Nakamura *et al.*[30] have reported that RTBM1, a human neuroblastoma cell line, is responsive to both BMP2 and RA by extending neurites. By using this system, we examined whether the expression levels of hTTL change during induction of neuronal differentiation. As shown in Figure 4, the treatment of RTBM1

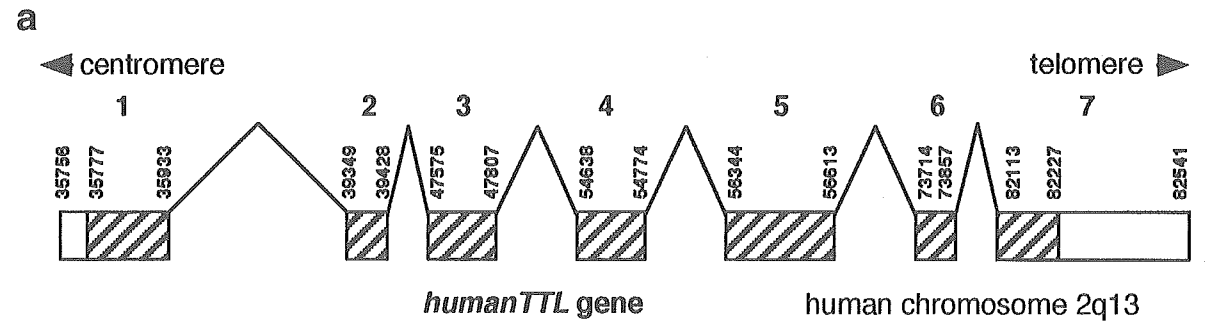

b

```
humanTTL  MYTFVVRDENSSVYAEVSRLLLATGHWKRLRRDNPRFNLMLGERNRLPFGRLGHEPGLVQLVNYYRGADKLCRKAS 76
mouseTTL  MYTFVVRDENSSVYAEVSRLLLATGYWKRLRRDNPRFNLMLGERNRLPFGRLGHEPGLAQLVNYYRGADKLCRKAS 76
ratTTL    MYTFVVRQENSSVYAEVSRLLLATGYWKRLRRDNPRFNLMLGGRNRLPFGRLGHEPGLAQLVNYYRGADKLCRKAS 76
pigTTL    MYTFVVRDENSSVYAEVSRLLLATGHWKRLRRDNPRFNLMLGERNRLPFGRLGHEPGLMQLVNYYRGADKLCRKAS 76
cowTTL    MYTFVVRDENSSVYAEVSRLLLATGHWKRLRRDNPRFNLMLGERNRLPFGRLGHEPGLMQLVNYYRGADKLCRKAS 76
          ******* ***************** ***************** *************** ****************

humanTTL  LVKLIKTSPELAESCTWFPESYVIYPTNLKTPVAPAQNGIQPPISNSRTDEREFFLASYNRKKEDGEGNVWIAKSS 152
mouseTTL  LVKLVKTSPELSESCSWFPESYVIYPTNLKTPVAPAQNGIQLPVSNSRTDEREFFLASYNRKKEDGEGNVWIAKSS 152
ratTTL    LVKLVKTSPELSESCSWFPESYVIHPTNLKTPVAPAQNGIQLPVSNSRTDEREFFLASYNRKKEDGEGNVWIAKSS 152
pigTTL    LVKLIKTSPELAESCTWFPESYVIYPTNLKTPVAPAQNGIHPPIHSSRTDEREFFLTSYNKKKEDGEGNVWIAKSS 152
cowTTL    LVKLIKTSPELAESCTWFPESYVIYPTNLKTPVAPAQDGIHPPLHSSRTDEREFFLASYNRKKEEGEGNVWIAKSS 152
          **** ****** *** ******** ************ ** *  ********** *** *** ************

humanTTL  AGAKGEGILISSEASELLDFIDNQGQVHVIQKYLEHPLLLEPGHRKFDIRSWVLVDHQYNIYLYREGVLRTASEPY 228
mouseTTL  AGAKGEGILISSEASELLDFIDSQGQVHVIQKYLERPLLLEPGHRKFDIRSWVLVDHQYNIYLYREGVLRTASEPY 228
ratTTL    AGAKGEGILISSEASELLDFIDNQGQVHVIQKYLEHPLLLEPGHRKFDIRSWVLVDHQYNIYLYREGVLRTASEPY 228
pigTTL    AGAKGEGILISSEATELLDFIDNQGQVHVIQKYLERPLLLEPGHRKFDIRSWVLVDHQYNIYLYREGVLRTASEPY 228
cowTTL    AGAKGEGILISSDATELLDFIDNQGQVHVIQKYLERPLLLEPGHRKFDIRSWVLVDHQFNIYLYREGVLRTASEPY 228
          ************ * ******* ************ ********************** ****************

humanTTL  HVDNFQDKTCHLTNHCIQKEYSKNYGKYEEGNEMFFKEFNQYLTSALNITLESSILLQIKHIIRNCLLSVEPAIST 304
mouseTTL  HVDNFQDKTCHLTNHCIQKEYSKNYGKYEEGNEMFFEEFNQYLTSALNITLESSILLQIKHIIRSCLMSVEPAIST 304
ratTTL    HVDNFQDKTCHLTNHCIQKEYSKNYGKYEEGNEMFFEEFNQYLTSALNITLENSILLQIKHIIRSCLMSVEPAIST 304
pigTTL    HTDNFQDKTCHLTNHCIQKEYSKNYGKYEEGNEMFFEEFNQYLTSALNITLESSILLQIKHIIRSCLLSVEPAIST 304
cowTTL    HMDNFQDKTCHLTNHCIQKEYSKNYGKYEEGNEMFFEAFNRYLTSALNITLESSILLQIKHIIRSCLMSVEPAIST 304
          * ********************************  ** *********** *********** ** ********

humanTTL  KHLPYQSFQLFGFDFMVDEELKVWLIEVNGAPACAQKLYAELCQGIVDIAISSVFPPPDVEQPQTQP--AAFIKL  377
mouseTTL  KHLPYQSFQLLGFDFMVDEELKVWLIEVNGAPACAQKLYAELCQGIVDIAISSVFPPPDTEQVPQQP--AAFVKL  377
ratTTL    KHLPYQSFQLLGFDFMVDEELKVWLIEVNGAPACAQKLYAELCQGIVDIAISSVFPPPDTEQVPQQP--AAFMKL  377
pigTTL    RHLPYQSFQLFGFDFMVDEDLKVWLIEVNGAPACAQKLYAELCQGIVDIAIASVFPPPDAEQQQQQPPPAAFIKL  379
cowTTL    KHLPYQSFQLFGFDFMVDEELKVWLIEVNGAPACAQKLYAELCQGIVDIAIASVFPPPDAEQQPPQP--ATFIKL  377
          ********* ******** ******************************** ******* **   **  * * **
```

c

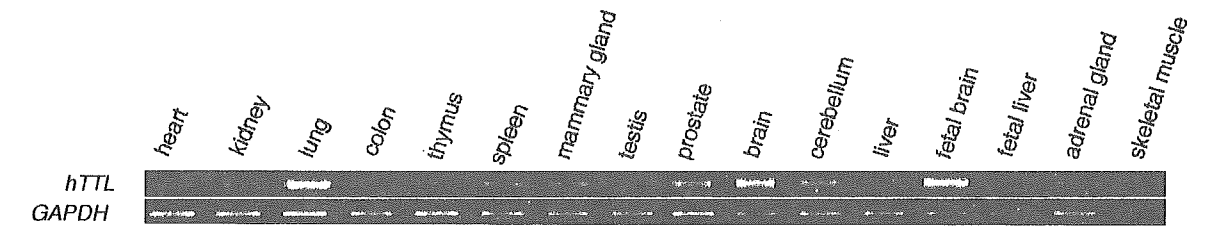

FIGURE 2

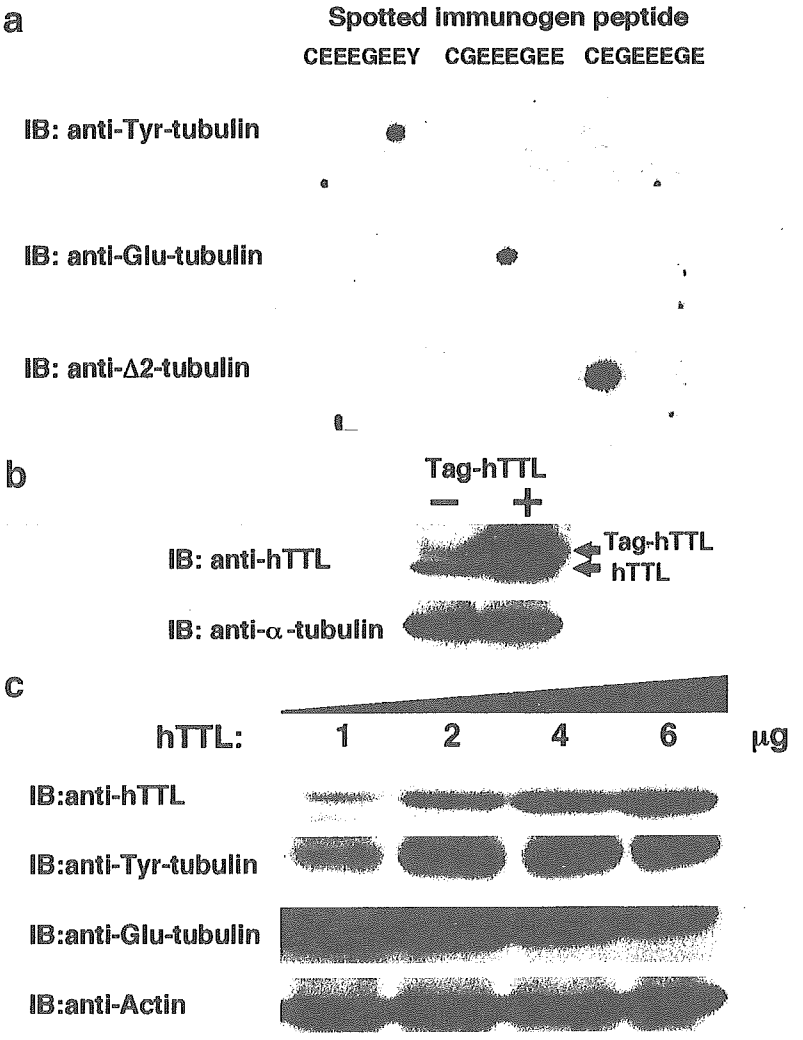

FIGURE 3 – hTTL has a tyrosination activity in mammalian cultured cells. (*a*) Specificity of antibodies. The indicated synthetic peptides were spotted on the filter and immunoblotted with the polyclonal anti-Tyr-tubulin (top), anti-Glu-tubulin (middle), or anti-Δ2-tubulin antibody (bottom). (*b*) Expression of FLAG-tagged hTTL. Whole-cell lysates prepared from COS7 cells transfected with the empty plasmid or with the expression plasmid for FLAG-tagged hTTL were subjected to immunoblotting with the anti-hTTL antibody (top). The expression level of α-tubulin was examined to ensure equal loading (bottom). (*c*) The exogenously expressed hTTL has a catalytic activity. HEK293T cells were transfected with increasing amounts of the hTTL expression plasmid. Forty-eight hours after transfection, whole-cell lysates were prepared and immunoblotted with the indicated antibodies. The expression level of actin is included as a loading control (bottom).

cells with 1 nM BMP2 or 5 μM RA induced remarkable morphologic differentiation by day 8. The hTTL protein level was increased after day 2 and peaked on day 6 in the former and on day 3 in the latter. Thereafter, it appeared to be decreased. Thus, hTTL was induced during induction of neuronal differentiation in NBL cells.

Expression of hTTL mRNA in primary neuroblastomas

To evaluate the clinical significance of *hTTL*, we examined the expression of *hTTL* mRNA in 16 favorable (stage 1, high expression of *TrkA* and a single copy of *MYCN*) and 16 unfavorable (stage 3 or 4, low expression of *TrkA* and amplification of *MYCN*) NBLs using semiquantitative RT-PCR. As shown in Figure 5(*a*), *hTTL* was preferentially expressed in favorable NBLs. Therefore, we next performed quantitative real-time RT-PCR to measure the levels of *hTTL* transcript in 74 primary NBLs. Table I shows the quantitative levels of *hTTL* mRNA expression (mean ± SEM) by age (< 1-year-old *vs.* ≥ 1-year-old), tumor stages (1 + 2 + 4s *vs.* 3 + 4), *TrkA* expression (low *vs.* high), *MYCN* gene copies (single *vs.* amplified), origin (adrenal gland *vs.* others), mass screening (tumors found by mass screening *vs.* sporadic tumors) and prognosis (alive *vs.* dead). High levels of *hTTL* expression were significantly associated with favorable stages ($p = 0.0069$), high *TrkA* expression ($p = 0.002$), a single copy of *MYCN* ($p < 0.00005$), tumors found by mass screening ($p = 0.0042$), origins other than adrenal gland ($p = 0.0042$) and a good prognosis ($p = 0.023$). *hTTL* expression was marginally associated with age. The log-rank test indicated that *hTTL* expression was associated with better survival ($p = 0.026$), which was also indicated in the Kaplan-Meier cumulative survival curves (Fig. 5*b*).

The univariate Cox regression was employed to examine the individual relationship of each variable to survival (Table II). Expression of *hTTL*, age, *MYCN* copy numbers and mass screening were found to be of prognostic importance, supporting the results of the log-rank test. However, since *hTTL* expression was highly associated with *MYCN*, mass screening and origin, multivariable Cox models were not fitted to assess the predictive importance of *hTTL* expression for survival after controlling these prognostic factors, suggesting that expression of *hTTL* was not an independent prognostic indicator.

FIGURE 2 – Genomic structure, alignment of amino acid sequence and mRNA expression of human *TTL*. (*a*) Genomic structure of *hTTL*. The *hTTL* gene that is mapped to 2q13 consists of 7 exons. Untranslated regions (open boxes) and coding regions (hatched boxes) are shown. Numbers indicate nucleotide position in human BAC clone *RP11-1I24* (accession number AC012442). (*b*) Comparison of amino acid sequences among mammalian TTLs. The gaps produced by the alignment are indicated by a hyphen in the sequence. The conserved amino acid residues in TTLs are shown by asterisks below the alignment. (*c*) Tissue distribution of *hTTL* mRNA. The expression levels of *hTTL* mRNA in the indicated human tissues were examined by semiquantitative RT-PCR (top). *GAPDH* expression was also examined as an internal control (bottom).

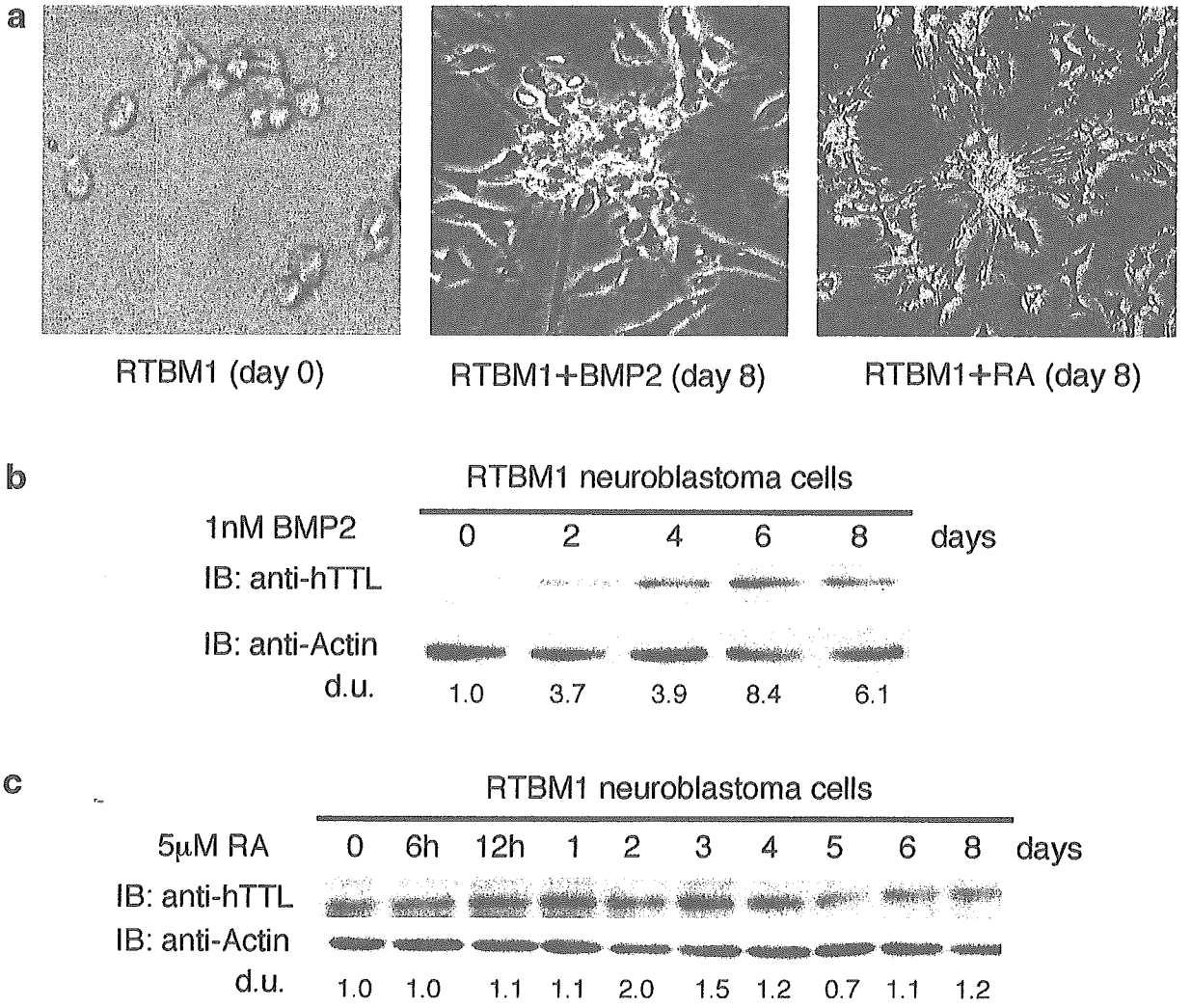

FIGURE 4 – TTL is induced during BMP2- and RA-mediated neuroblastoma differentiation. (*a*) BMP2- or RA-induced morphologic changes in RTBM1 neuroblastoma cells. RTBM1 cells were treated with BMP2 or RA at a final concentration of 1 nM or 5 μM, respectively, and maintained for 8 days. (*b*) Expression levels of hTTL are increased in response to BMP2. At the indicated time points after the treatment with BMP2 (at a final concentration of 1 nM), whole-cell lysates prepared from RTBM1 cells were subjected to immunoblotting with the antibody against hTTL (top). Actin protein levels were determined as a loading control (bottom). (*c*) Induction of hTTL in response to RA. RTBM1 cells were exposed to RA at a final concentration of 5 μM. Whole-cell lysates were prepared at the indicated time points after the treatment with RA and subjected to immunoblotting with the anti-hTTL (top) or with antiactin (bottom) antibody. d.u., arbitrary density units.

Immunohistochemistry

To determine the expression pattern of hTTL protein in primary NBLs, we performed immunohistochemical study for 6 favorable (stage 1 or 2 and a single copy of *MYCN*) and 4 unfavorable (stage 3 or 4 and amplified *MYCN*) NBLs. hTTL, Tyr-tubulin and Glu-tubulin were positively detected both in the cytoplasm of the neuroblastic cells and in the fine meshwork of neuropil of all 6 tumors with favorable histology (Shimada's classification) and a single copy of *MYCN* (Fig. 6*a–c*). In contrast, all 4 tumors with unfavorable histology and *MYCN* amplification were negative for Tyr-tubulin and Glu-tubulin, and only 1 tumor in this subset was positive for hTTL (Fig. 6*f–h*). Interestingly, all 10 NBL tumors were positive for Δ2-tubulin, but whose staining pattern was rather distinct in different subsets of the tumors. In the favorable tumors, Δ2-tubulin showed a localization similar to hTTL, Tyr-tubulin and Glu-tubulin and was detected in the cytoplasm and in the fine neuropil (Fig. 6*d*). On the other hand, Δ2-tubulin in the aggressive tumors was found only in the cytoplasm of neuroblastic cells, since they had no or a very limited capability of neuritic process production (*i.e.*, neuropil formation; Fig. 6*i*).

CD56 was detected in all 10 tumors, regardless of the histology and *MYCN* status (data not shown). TrkA was detected in all of 6 favorable tumors (Fig. 6*e*), but was negative in 3 of 4 aggressive tumors (Fig. 6*j*). It was noted that one unfavorable tumor with weakly positive trkA showed positive staining for TTL. Ki-67 staining revealed 10–20% and 60–70% positive cells in the favorable and the unfavorable tumors, respectively (data not shown).

DISCUSSION

In the present study, we have identified human ortholog of *tubulin tyrosine ligase* gene, which is highly conserved among the mammalian species. *hTTL* mRNA is ubiquitously expressed but rather preferential in both fetal and adult brains as well as in lung. The specific antibodies raised against hTTL, Tyr-tubulin, Glu-tubulin and Δ2-tubulin have confirmed the catalytic activity of

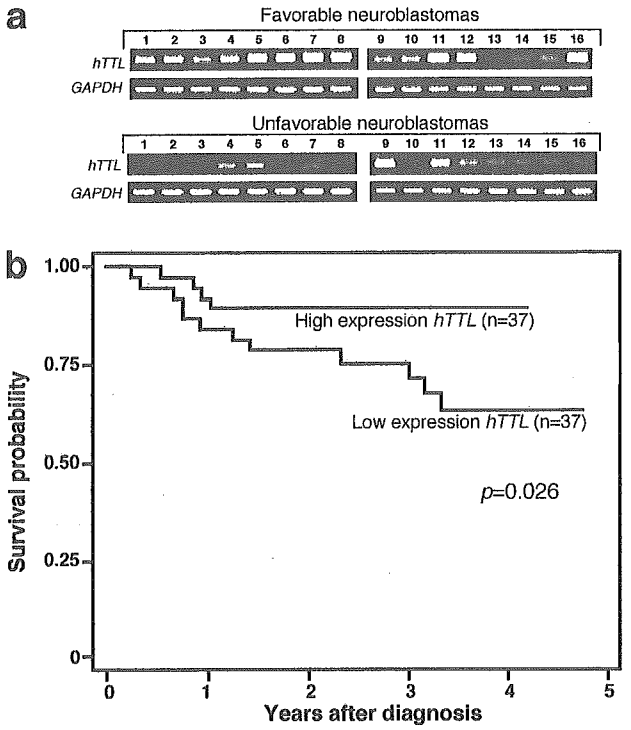

FIGURE 5 – Expression of *hTTL* mRNA is associated with unfavorable prognosis of neuroblastoma. (*a*) Total RNA was purified from the indicated favorable (top) and unfavorable NBL tissues (bottom) and subjected to semiquantitative RT-PCR. Sixteen favorable cases used in this study were classified as stage 1 NBL with a single copy *MYCN* as well as a high expression of *TrkA*. Sixteen unfavorable cases were in stages 3 and 4 NBL with *MYCN* amplification as well as a low *TrkA* expression. *GAPDH* expression was also examined as an internal control. (*b*) Association of *hTTL* mRNA expression levels with favorable prognosis of NBL. Total RNA was prepared from 74 NBL tissues, and *hTTL* mRNA levels were assayed by quantitative real-time RT-PCR as described in text. The values of *hTTL* mRNA were normalized by *GAPDH*. The survival of *hTTL* relatively high-expression group (n = 37) and *hTTL* low-expression group (n = 37) was compared using the Kaplan-Meier procedure.

TABLE I – RESULTS OF LOG-RANK TESTS FOR CONVENTIONAL PROGNOSTIC FACTORS AND EXPRESSION OF *hTTL* IN 74 PRIMARY NEUROBLASTOMAS

Variable	n	*hTTL* expression[1]	p-value
Age (year)			0.1
<1	43	117 ± 14	
≥1	31	77 ± 10	
Tumor stage			0.0069
1, 2, 4s	40	127 ± 14	
3, 4	34	69 ± 9	
TrkA expression			0.002
High	36	125 ± 17	
Low	38	77 ± 8	
MYCN			<0.00005
Single	52	123 ± 11	
Amplified	22	46 ± 9	
Mass screening			0.0042
+	37	128 ± 14	
−	37	72 ± 10	
Origin			0.0042
Adrenal gland	47	85 ± 11	
Others	27	127 ± 16	
Prognosis			0.023
Alive	58	113 ± 11	
Dead	16	54 ± 11	

[1]Mean ± SEM.

TABLE II – COX REGRESSION MODELS USING DICHOTOMOUS FACTORS OF AGE, *MYCN* AMPLIFICATION, MASS SCREENING, ORIGIN AND EXPRESSION OF *hTTL*

Factor	p-value	Hazard ratio (95% confidence interval)
hTTL expression (log)	0.024	0.64 (0.44, 0.94)
Age (> 1 *vs.* < 1 year)	0.005	5.04 (1.61, 15.8)
MYCN (1 copy *vs.* > 1 copy)	<0.0005	0.06 (0.017, 0.22)
Mass screening (+ *vs.* −)	0.004	0.05 (0.007, 0.38)
Origin (adrenal gland *vs.* others)	0.31	1.79 (0.58, 5.57)

hTTL encoded by the *hTTL* gene in the cells. Interestingly, hTTL is induced during neurite extension in RTBM1 NBL cells treated with BMP2 or RA, suggesting that hTTL expression is associated with neuronal differentiation in human NBL. Immunohistochemically, favorable NBLs are positive for hTTL, Tyr-tubulin, Glu-tubulin and Δ2-tubulin, whereas unfavorable tumors with *MYCN* amplification are positive only for Δ2-tubulin, suggesting that deregulation of tyrosination/detyrosination cycle contributes to malignant progression of NBL. This hypothesis has been further supported by a significant decrease of the levels of *hTTL* expression in the patients with poor prognosis.

The dynamics of microtubule regulates many cellular functions, including migration, motility, differentiation, cell division and cellular cap formation. Though posttranslational modifications of tubulin and their enzymatic regulation have long been studied, the precise mechanisms are still largely unknown. It is interesting that no orthologs of highly conserved mammalian TTL have so far been reported in *Caenorhabditis elegans*, *Drosophila melanogaster* and *Saccharomyces cerevisiae*, suggesting that the tyrosination/detyrosination cycle of tubulin may be related to evolution of the cellular functions, including neuronal differentiation. In newborn rats, TTL expression is found in skeletal muscle at high levels and is developmentally regulated by rapidly decreasing its level during early postnatal period.[31] It is interesting that both BMP2 and RA, which have increased levels of hTTL expression, function as regulators to induce differentiation during neural development.

The tyrosination/detyrosination of tubulin may be regulated by the activities of both TTL and tubulin carboxypeptidase (TCP). Until now, however, the *TCP* gene has never been identified in vertebrates, although biochemical TCP activity has been reported to be present in some subcellular fractions.[18] Tubulin is also posttranslationally modified by nitrotyrosination. Eiserich *et al.*[32] showed that free 3-nitrotyrosine (NO_2Tyr) is transported into mammalian cells and selectively incorporated into the Glu-tubulin posttranslationally, which is catalyzed by TTL. Cellular injury such as microtubule disorganization has consequently been induced. Kalisz *et al.*[33] also showed that nitrotyrosine can be incorporated into α-tubulin by *in vitro* assays. Those reports demonstrated that carboxypeptidase A is incapable of cleaving nitrotyrosine from the modified α-tubulin. On the other hand, Bisig *et al.*[34] reported that nitrotyrosinated tubulin is a good substrate of physiologic TCP, and that it has a similar capability to that of the tyrosinated tubulin to assemble into microtubules, suggesting that incorporation of nitrotyrosine is not injurious at least to dividing cells. Therefore, whether nitrotyrosinated tubulin is harmful or not is still controversial. Nevertheless, as increased nitrotyrosination is reported in Alzheimer's disease and amyotrophic lateral sclerosis,[35–37] the functional analysis of the role of hTTL and tubulin tyrosination/detyrosination cycle should be important for understanding the pathogenesis of these disease. The treatment of cells with methylmercury (MeHg) is also reported to induce perturbation of cellular activities associated with the tubulin/microtubule system by altering the status of tubulin tyrosination in the rat

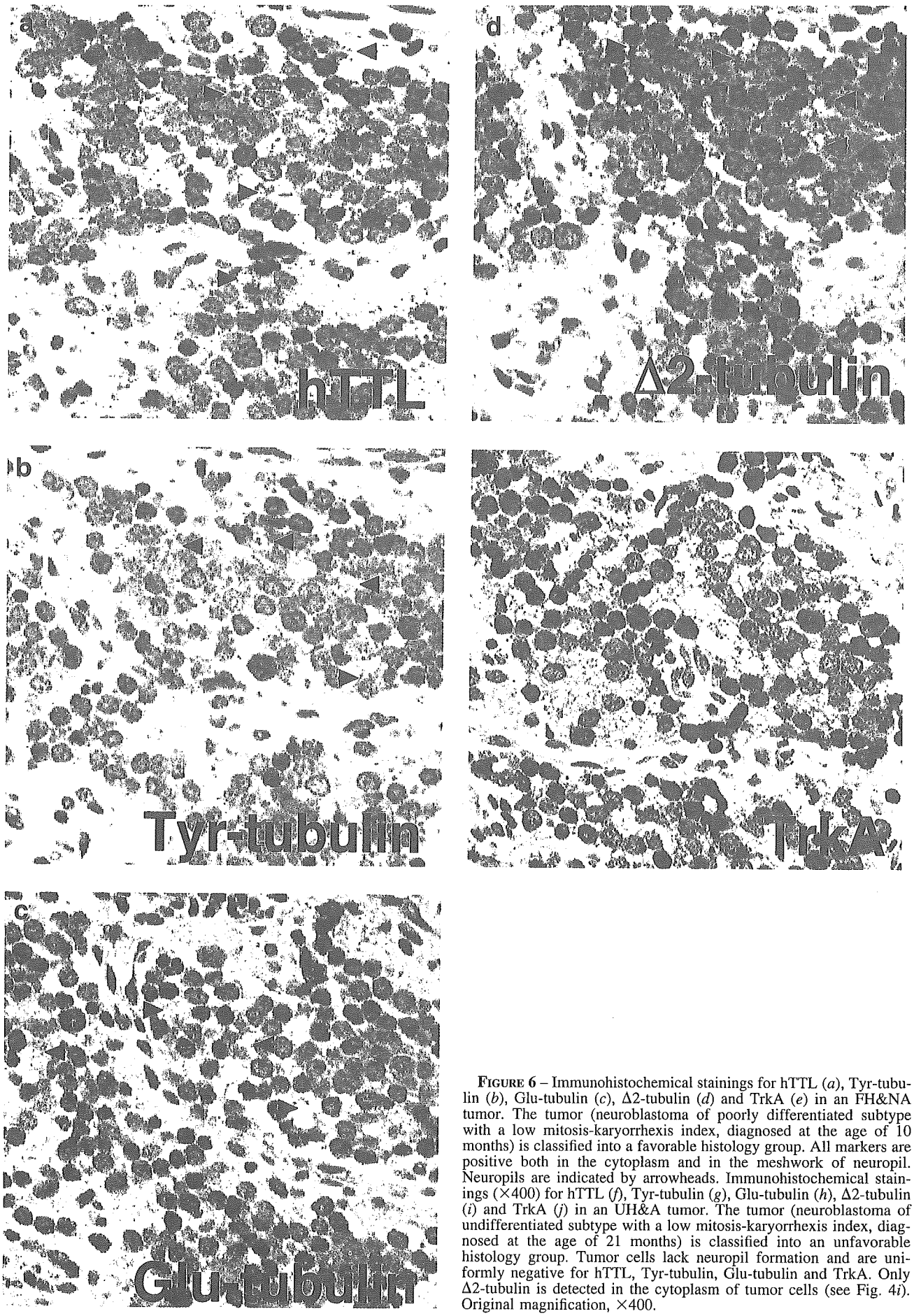

FIGURE 6 – Immunohistochemical stainings for hTTL (*a*), Tyr-tubulin (*b*), Glu-tubulin (*c*), Δ2-tubulin (*d*) and TrkA (*e*) in an FH&NA tumor. The tumor (neuroblastoma of poorly differentiated subtype with a low mitosis-karyorrhexis index, diagnosed at the age of 10 months) is classified into a favorable histology group. All markers are positive both in the cytoplasm and in the meshwork of neuropil. Neuropils are indicated by arrowheads. Immunohistochemical stainings (×400) for hTTL (*f*), Tyr-tubulin (*g*), Glu-tubulin (*h*), Δ2-tubulin (*i*) and TrkA (*j*) in an UH&A tumor. The tumor (neuroblastoma of undifferentiated subtype with a low mitosis-karyorrhexis index, diagnosed at the age of 21 months) is classified into an unfavorable histology group. Tumor cells lack neuropil formation and are uniformly negative for hTTL, Tyr-tubulin, Glu-tubulin and TrkA. Only Δ2-tubulin is detected in the cytoplasm of tumor cells (see Fig. 4*i*). Original magnification, ×400.

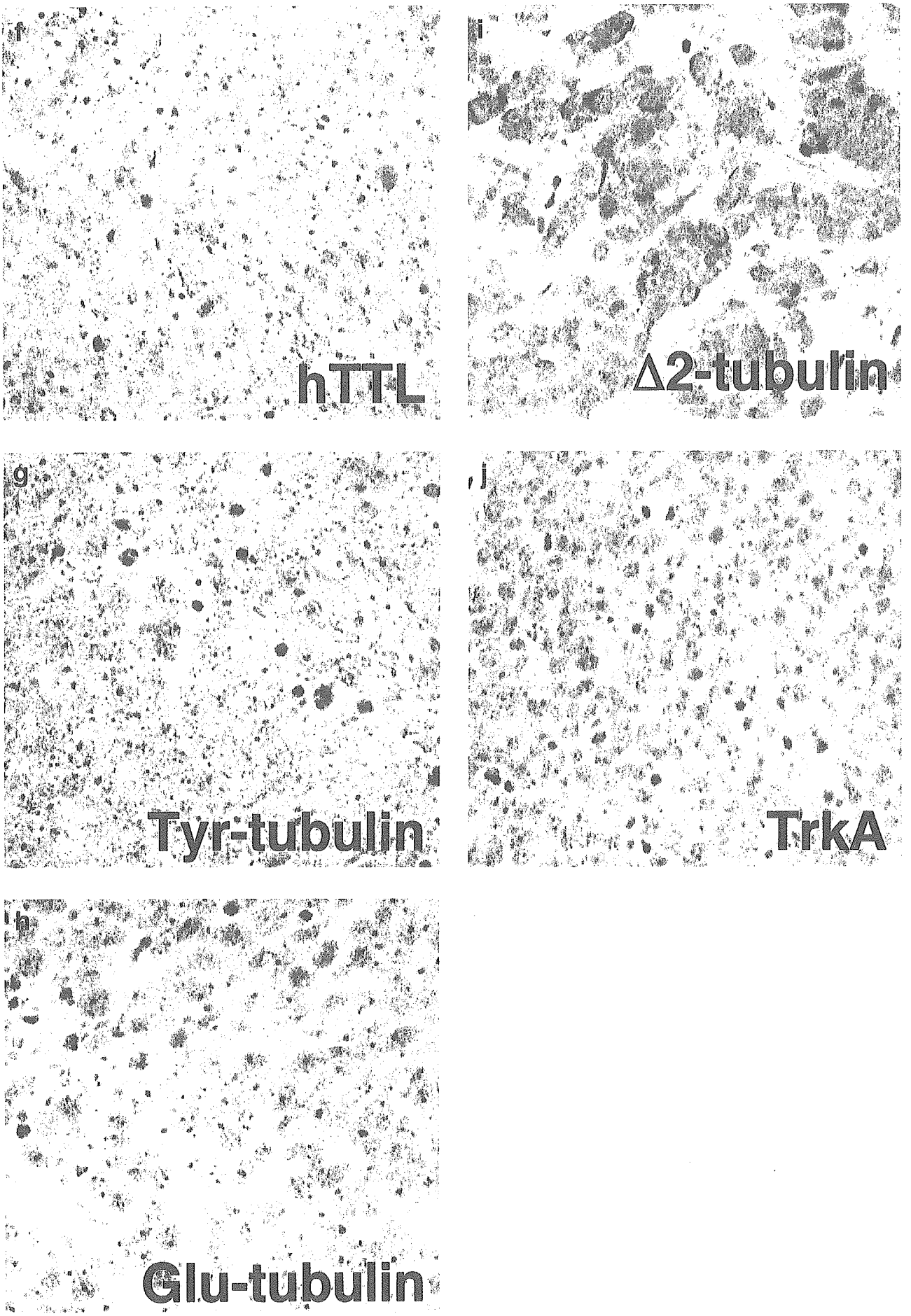

FIGURE 6 – (CONTINUED)

brain.[38] Therefore, many cellular stresses such as oxidative damage may trigger dysfunction of the tubulin/microtubule cytoskeletal system.

Our present study has shown that the decreases in Tyr-tubulin and Glu-tubulin are associated with relatively low levels of hTTL expression in unfavorable NBLs, which have lost a potency of neuronal differentiation and/or apoptosis. They are also correlated with decreased levels of TrkA, a high-affinity receptor for nerve growth factor, whose activation induces morphologic differentiation of NBL cells.[39] In addition, gradual upregulation of hTTL has been observed during induction of neuronal differentiation in RTBM1 cells treated with BMP2 or RA. These suggest that the induction of neuronal differentiation in NBL is accompanied with the activated tyrosination/detyrosination cycle regulated by increased level of hTTL enzyme, while the cycle is arrested by downregulation of hTTL in proliferating NBL cells, resulting in accumulation of Δ2-tubulin within the cells. Indeed, the expression levels of *hTTL* mRNA and Δ2-tubulin are significantly correlated with the prognosis of primary NBLs. This is consistent with the observation that TTL activity is lost, and conversely Δ2-tubulin is upregulated during the tumor cell growth.[19] Lafanechere *et al.*[19] have demonstrated by using mouse TTL null cells both *in vitro* and *in vivo* that mouse TTL activity is strongly decreased during tumor growth. Mas *et al.*[15] have also reported that, using rat *TTL* dominant negative mutant and an antisense cDNA of rat *TTL*, suppression of TTL activity induces 2- to 3-fold faster cell proliferation. Moreover, in human breast cancers, the accumulation of Glu-tubulin and Δ2-tubulin is correlated with poor prognosis by immunohistochemical approach.[28] It is noteworthy that our preliminary data using the microarray hybridized with total RNA obtained from 136 primary NBLs have shown that the gene with the highest score to predict prognosis of NBLs is α-tubulin (data not shown). Thus, the role of microtubule and its component, α-tubulin, is very important to define the biology as well as the aggressiveness of cancer cells.

In conclusion, we have identified a *human tubulin tyrosine ligase* gene and demonstrated its tissue distribution and correlation with neuronal differentiation. Since our data have suggested that the tyrosination cycle of α-tubulin is activated in differentiating NBLs but is inactivated in proliferating tumors, the cycle-related molecules including hTTL could be the targets for developing novel therapeutic strategies against advanced stages of NBL.

ACKNOWLEDGEMENTS

The authors thank Shigeru Sakiyama for critical reading of the manuscript, Naoko Sugimitsu for preparing RNA, Yuki Nakamura for DNA sequencing, Yoshiaki Okamoto for instructing quantitative real-time RT-PCR and Aiko Morohashi and Natsue Akao for technical assistance. The authors also thank the following institutions for providing surgical samples: First Department of Surgery, Hokkaido University School of Medicine; Department of Pediatrics, National Sapporo Hospital; Department of Pediatric Surgery, Tohoku University School of Medicine; Department of Surgery, Gunma Children's Medical Center; Department of Pediatrics, Pediatric Surgery and General Surgery, Jichi Medical University; Department of Hematology and Oncology, Saitama Children's Medical Center; Department of Pediatrics, Juntendo University School of Medicine; Department of Surgery, Kiyose Metropolitan Children's Hospital; Department of Surgery and Pathology, Chiba Children's Hospital; Department of Pediatric Surgery, Chiba University School of Medicine; Department of Pediatric Surgery, Kimitsu Central Hospital; Department of Pediatric Surgery, Niigata University School of Medicine; Department of Pediatrics and Pediatric Surgery, Aichi Medical University; Department of Pediatrics, Kyoto Prefectural Medical University; Tumor Board, Hyogo Children's Hospital; Department of Pediatrics and Pediatric Surgery, Kagoshima University School of Medicine; Department of Pediatric Surgery, Showa University School of Medicine; Department of Pediatrics, Oita University School of Medicine; Department of Pediatric Surgery, Ohta General Hospital; Department of Pediatrics, Ichinomiya City Hospital; Department of Pediatric Surgery, Osaka City General Hospital; Department of Pediatrics, Nihon University School of Medicine; Itabashi Hospital; Department of Pediatric Surgery, University of Tsukuba School of Medicine.

REFERENCES

1. MacRae TH. Tubulin post-translational modifications: enzymes and their mechanisms of action. Eur J Biochem 1997;244:265–78.
2. Zambito AM, Wolff J. Palmitoylation of tubulin. Biochem Biophys Res Commun 1997;239:650–4.
3. Barra HS, Arce CA, Argarana CE. Posttranslational tyrosination/detyrosination of tubulin. Mol Neurobiol 1988;2:133–53.
4. Luduena RF. Multiple forms of tubulin: different gene products and covalent modifications. Int Rev Cytol 1998;178:207–75.
5. Barra HS, Unates LE, Sayavedra MS, Caputto R. Capacities for binding amino acids by tRNAs from rat brain and their changes during development. J Neurochem 1972;19:2289–97.
6. Barra HS, Rodriguez JA, Arce CA, Caputto R. A soluble preparation from rat brain that incorporates into its own proteins (14 C)arginine by a ribonuclease-sensitive system and (14 C)tyrosine by a ribonuclease-insensitive system. J Neurochem 1973;20:97–108.
7. Barra HS, Arce CA, Rodriguez JA, Caputto R. Incorporation of phenylalanine as a single unit into rat brain protein: reciprocal inhibition by phenylalanine and tyrosine of their respective incorporations. J Neurochem 1973;21:1241–51.
8. Barra HS, Arce CA, Rodriguez JA, Caputto R. Some common properties of the protein that incorporates tyrosine as a single unit and the microtubule proteins. Biochem Biophys Res Commun 1974;60:1384–90.
9. Arce CA, Rodriguez JA, Barra HS, Caputo R. Incorporation of L-tyrosine, L-phenylalanine and L-3,4-dihydroxyphenylalanine as single units into rat brain tubulin. Eur J Biochem 1975;59:145–9.
10. Argarana CE, Arce CA, Barra HS, Caputto R. *In vivo* incorporation of [14C]tyrosine into the C-terminal position of the alpha subunit of tubulin. Arch Biochem Biophys 1977;180:264–8.
11. Preston SF, Deanin GG, Hanson RK, Gordon MW. The phylogenetic distribution of tubulin:tyrosine ligase. J Mol Evol 1979;13:233–44.
12. Gabius HJ, Graupner G, Cramer F. Activity patterns of aminoacyl-tRNA synthetases, tRNA methylases, arginyltransferase and tubulin: tyrosine ligase during development and ageing of *Caenorhabditis elegans*. Eur J Biochem 1983;131:231–4.
13. Stieger J, Wyler T, Seebeck T. Partial purification and characterization of microtubular protein from *Trypanosoma brucei*. J Biol Chem 1984;259:4596–602.
14. Ersfeld K, Wehland J, Plessmann U, Dodemont H, Gerke V, Weber K. Characterization of the tubulin-tyrosine ligase. J Cell Biol 1993;120:725–32.
15. Mas CR, Arregui CO, Filiberti A, Argarana CE, Barra HS. Cloning of rat olfactory bulb tubulin tyrosine ligase cDNA: a dominant negative mutant and an antisense cDNA increase the proliferation rate of cells in culture. Neurochem Res 2002;27:1453–8.
16. Paturle-Lafanechere L, Edde B, Denoulet P, Van Dorsselaer A, Mazarguil H, Le Caer JP, Wehland J, Job D. Characterization of a major brain tubulin variant which cannot be tyrosinated. Biochemistry 1991;30:10523–8.
17. Paturle-Lafanechere L, Manier M, Trigault N, Pirollet F, Mazarguil H, Job D. Accumulation of delta 2-tubulin, a major tubulin variant that cannot be tyrosinated, in neuronal tissues and in stable microtubule assemblies. J Cell Sci 1994;107:1529–43.
18. Lafanechere L, Job D. The third tubulin pool. Neurochem Res 2000;25:11–8.
19. Lafanechere L, Courtay-Cahen C, Kawakami T, Jacrot M, Rudiger M, Wehland J, Job D, Margolis RL. Suppression of tubulin tyrosine ligase during tumor growth. J Cell Sci 1998;111:171–81.
20. Ohira M, Morohashi A, Inuzuka H, Shishikura T, Kawamoto T, Kageyama H, Nakamura Y, Isogai E, Takayasu H, Sakiyama S, Suzuki Y, Sugano S, Goto T, Sato S, Nakagawara A. Expression profiling and characterization of 4200 genes cloned from primary neuroblastomas: identification of 305 genes differentially expressed between favorable and unfavorable subsets. Oncogene 2003;22:5525–36.
21. Ohira M, Morohashi A, Nakamura Y, Isogai E, Furuya K, Hamano S, Machida T, Aoyama M, Fukumura M, Miyazaki K, Suzuki Y, Sugano S, Hirato J, Nakagawara A. Neuroblastoma oligo-capping cDNA

project: toward the understanding of the genesis and biology of neuroblastoma. Cancer Lett 2003;197:63–8.
22. Brodeur GM, Pritchard J, Berthold F, Carlsen NL, Castel V, Castelberry RP, De Bernardi B, Evans AE, Favrot M, Hedborg F, kaneko M, Kemshead J, Lampert F, Lee RE, Look AT, Pearson AD, Philip T, Roald B, Sawada T, Seeger RC, Thuchida Y, Voute PA. Revisions of the international criteria for neuroblastoma diagnosis, staging, and response to treatment. J Clin Oncol 1993;11:1466–77.
23. Kaneko M, Nishihira H, Mugishima H, Ohnuma N, Nakada K, Kawa K, Fukuzawa M, Suita S, Sera Y, Tsuchida Y. Stratification of treatment of stage 4 neuroblastoma patients based on N-myc amplification status: Study Group of Japan for Treatment of Advanced Neuroblastoma, Tokyo, Japan. Med Pediatr Oncol 1998;31:1–7.
24. Hishiki T, Nimura Y, Isogai E, Kondo K, Ichimiya S, Nakamura Y, Ozaki T, Sakiyama S, Hirose M, Seki N, Takahashi H, Ohnuma N, Tanabe M, Nakagawara A. Glial cell line-derived neurotrophic factor/neurturin-induced differentiation and its enhancement by retinoic acid in primary human neuroblastomas expressing c-Ret, GFR alpha-1, and GFR alpha-2. Cancer Res 1998;58:2158–65.
25. Chomczynski P, Sacchi N. Single-step method of RNA isolation by acid guanidinium thiocyanate-phenol-chloroform extraction. Anal Biochem 1987;162:156–9.
26. Shimada H, Ambros IM, Dehner LP, Hata J, Joshi VV, Roald B, Stram DO, Gerbing RB, Lukens JN, Matthay KK, Castleberry RP. The International Neuroblastoma Pathology Classification (the Shimada system). Cancer 1999;86:364–72.
27. Goto S, Umehara S, Gerbing RB, Stram DO, Brodeur GM, Seeger RC, Lukens JN, Matthay KK, Shimada H. Histopathology (International Neuroblastoma Pathology Classification) and MYCN status in patients with peripheral neuroblastic tumors: a report from the Children's Cancer Group. Cancer 2001;92:2699–708.
28. Mialhe A, Lafanechere L, Treilleux I, Peloux N, Dumontet C, Bremond A, Panh MH, Payan R, Wehland J, Margolis RL, Job D. Tubulin detyrosination is a frequent occurrence in breast cancers of poor prognosis. Cancer Res 2001;61:5024–7.
29. Iwasaki S, Hattori A, Sato M, Tsujimoto M, Kohno M. Characterization of the bone morphogenetic protein-2 as a neurotrophic factor: induction of neuronal differentiation of PC12 cells in the absence of mitogen-activated protein kinase activation. J Biol Chem 1996;271:17360–5.
30. Nakamura Y, Ozaki T, Koseki H, Nakagawara A, Sakiyama S. Accumulation of p27 KIP1 is associated with BMP2-induced growth arrest and neuronal differentiation of human neuroblastoma-derived cell lines. Biochem Biophys Res Commun 2003;307:206–13.
31. Arregui CO, Mas CR, Argarana CE, Barra HS. Tubulin tyrosine ligase: protein and mRNA expression in developing rat skeletal muscle. Dev Growth Differ 1997;39:167–78.
32. Eiserich JP, Estevez AG, Bamberg TV, Ye YZ, Chumley PH, Beckman JS, Freeman BA. Microtubule dysfunction by posttranslational nitrotyrosination of alpha-tubulin: a nitric oxide-dependent mechanism of cellular injury. Proc Natl Acad Sci USA 1999;96:6365–70.
33. Kalisz HM, Erck C, Plessmann U, Wehland J. Incorporation of nitrotyrosine into alpha-tubulin by recombinant mammalian tubulin-tyrosine ligase. Biochim Biophys Acta 2000;1481:131–8.
34. Bisig CG, Purro SA, Contin MA, Barra HS, Arce CA. Incorporation of 3-nitrotyrosine into the C-terminus of alpha-tubulin is reversible and not detrimental to dividing cells. Eur J Biochem 2002;269:5037–45.
35. Ischiropoulos H. Biological tyrosine nitration: a pathophysiological function of nitric oxide and reactive oxygen species. Arch Biochem Biophys 1998;3561–611.
36. Hensley K, Maidt ML, Yu Z, Sang H, Markesbery WR, Floyd RA. Electrochemical analysis of protein nitrotyrosine and dityrosine in the Alzheimer brain indicates region-specific accumulation. J Neurosci 1998;18:8126–32.
37. Beal MF, Ferrante RJ, Browne SE, Matthews RT, Kowall NW, Brown RH Jr. Increased 3-nitrotyrosine in both sporadic and familial amyotrophic lateral sclerosis. Ann Neurol 1997;42:644–54.
38. Ishida Y, Ichimura T, Sumi H, Horigome T, Omata S. Methylmercury alters the tyrosination status of tubulin in the brains of acutely intoxicated rats. Toxicology 1997;122:171–81.
39. Nakagawara A, Arima-Nakagawara M, Scavarda NJ, Azar CG, Cantor AB, Brodeur GM. Association between high levels of expression of the TRK gene and favorable outcome in human neuroblastoma. N Engl J Med 1993;328:847–54.

CpG Island Methylator Phenotype Is a Strong Determinant of Poor Prognosis in Neuroblastomas

Masanobu Abe,[1,2] Miki Ohira,[3] Atsushi Kaneda,[1] Yukiko Yagi,[1] Seiichiro Yamamoto,[4] Yoshihiro Kitano,[5] Tsuyoshi Takato,[2] Akira Nakagawara,[3] and Toshikazu Ushijima[1]

[1]Carcinogenesis Division, National Cancer Center Research Institute; [2]Department of Oral and Maxillo Facial Surgery, University of Tokyo Graduate School of Medicine; [3]Biochemistry Division, Chiba Cancer Center Research Institute; [4]Information Division, Research Center for Cancer Prevention and Screening, National Cancer Center; and [5]Department of Pediatric Surgery, National Center for Child Health and Development, Tokyo, Japan

Abstract

Neuroblastoma, one of the most common pediatric solid tumors, is characterized by two extreme disease courses, spontaneous regression and life-threatening progression. Here, we conducted a genome-wide search for differences in DNA methylation that distinguish between neuroblastomas of the two types. Three CpG islands (CGI) and two groups of CGIs were found to be methylated specifically in neuroblastomas with a poor prognosis. By quantitative analysis of 140 independent cases, methylation of all the five CGI (groups) was shown to be closely associated with each other, conforming to the CpG island methylator phenotype (CIMP) concept. The presence of CIMP was sensitively detected by methylation of the *PCDHB* CGIs and associated with significantly poor survival (hazard ratio, 22.1; 95% confidence interval, 5.3-93.4; $P < 0.0001$). Almost all cases with N-*myc* amplification (37 of 38 cases) exhibited CIMP. Even in 102 cases without N-*myc* amplification, the presence of CIMP (30 cases) strongly predicted poor survival (hazard ratio, 12.4; 95% confidence interval, 2.6-58.9; $P = 0.002$). Methylation of *PCDHB* CGIs, located in their gene bodies, did not suppress gene expression or induce histone modifications. However, CIMP was significantly associated with methylation of promoter CGIs of the *RASSF1A* and *BLU* tumor suppressor genes. The results showed that neuroblastomas with CIMP have a poor prognosis and suggested induction of silencing of important genes as an underlying mechanism. (Cancer Res 2005; 65(3): 828-34)

Introduction

Epigenetic abnormalities, especially alterations in DNA methylation, are intimately involved in development of various human tumors (1). Aberrant methylation of promoter CpG islands (CGI) causes inactivation of tumor suppressor genes. Genomic instability is caused by genomic hypomethylation and is associated with hypermethylation (2, 3). Identification of epigenetic abnormalities in human cancers is expected to lead not only to discovery of novel disease mechanisms but also to development of new diagnostic markers. Therefore, we previously developed a genome-wide scanning method, methylation-sensitive representational difference analysis (MS-RDA), for detecting differences in DNA methylation (4, 5). This technique analyzes unmethylated, CpG-rich regions of the genome and has already identified genes silenced in human lung, stomach, breast, and pancreatic cancers (6–9).

Neuroblastoma derived from primitive cells of the sympathetic nervous system is one of the most common solid tumors in childhood, characterized by two extreme disease courses, spontaneous regression, and life-threatening progression (10, 11). The clinical outcome is associated with disease stage, age at diagnosis, histologic classification, N-*myc* amplification, DNA ploidy, and *TrkA* overexpression (10–12). These characteristics are therefore used to classify cases into low-, intermediate-, and high-risk groups. However, especially in the cases with intermediate risk, prediction of prognosis and therapeutic decision-making are still difficult, and development of new markers is an urgent priority. Moreover, the molecular bases underlying the two distinct clinical courses are still unknown, and their clarification is needed to allow development of novel therapeutics.

In the present study, considering the major involvement of epigenetic machinery in embryonic development (13, 14), we searched for differences in DNA methylation between neuroblastomas with a good prognosis and counterparts with a poor prognosis by MS-RDA.

Materials and Methods

Tissue Samples and Cell Lines. Tumor samples were obtained from 145 nonrecurrent cases between 1995 and 1999 and were used under approval of institutional review boards. The mean age at initial diagnosis was 27 months (range, 0-216 months). Their clinical stages were determined according to the International Neuroblastoma Staging System, and 40, 17, 20, 60, and 8 cases belonged to stages I, II, III, IV, and IVS, respectively. Normal adrenal medulla tissue was collected from a case undergoing nephrectomy for a renal cancer. Neuroblastoma cell lines were obtained from the American Type Culture Collection (Manassas, VA), the Japanese Collection of Research Bioresources (Tokyo, Japan), and the RIKEN Bio Resource Center (Tsukuba, Japan). GANB was established by A.N. and normal human bronchial epithelial cells were purchased from Cambrex (East Rutherford, NJ). High molecular weight DNA and total RNA were extracted as previously described (7). Total RNAs of brain and adrenal glands were purchased from Clontech (Palo Alto, CA).

MS-RDA and Database Search. MS-RDA was done as previously described (4, 5). Genomic DNA of primary neuroblastomas with a good prognosis (cases 92, 98, 104, 112, and 148) and neuroblastoma cell lines established from cases with a poor prognosis (CHP134, IMR32, GANB, NGP, and TGW) were digested with *Hpa*II, and then two pooled DNA samples were prepared. Although use of cell lines is highly recommended for MS-RDA (5), no cell lines were available for neuroblastomas with a good prognosis, and therefore we used the primary samples. To isolate CGIs that were hypermethylated in the latter, the cell line pool was used as the tester, and the primary tumor pool as the driver. MS-RDA in the opposite direction

Note: Supplementary data for this article are available at Cancer Research online (http://cancerres.aacrjournals.org/).

Requests for reprints: Toshikazu Ushijima, 5-1-1 Tsukiji, Chuo-ku, Tokyo 104-0045, Japan. Phone: 133-547-5240; Fax: 135-565-1753; E-mail: tushijim@ncc.go.jp.

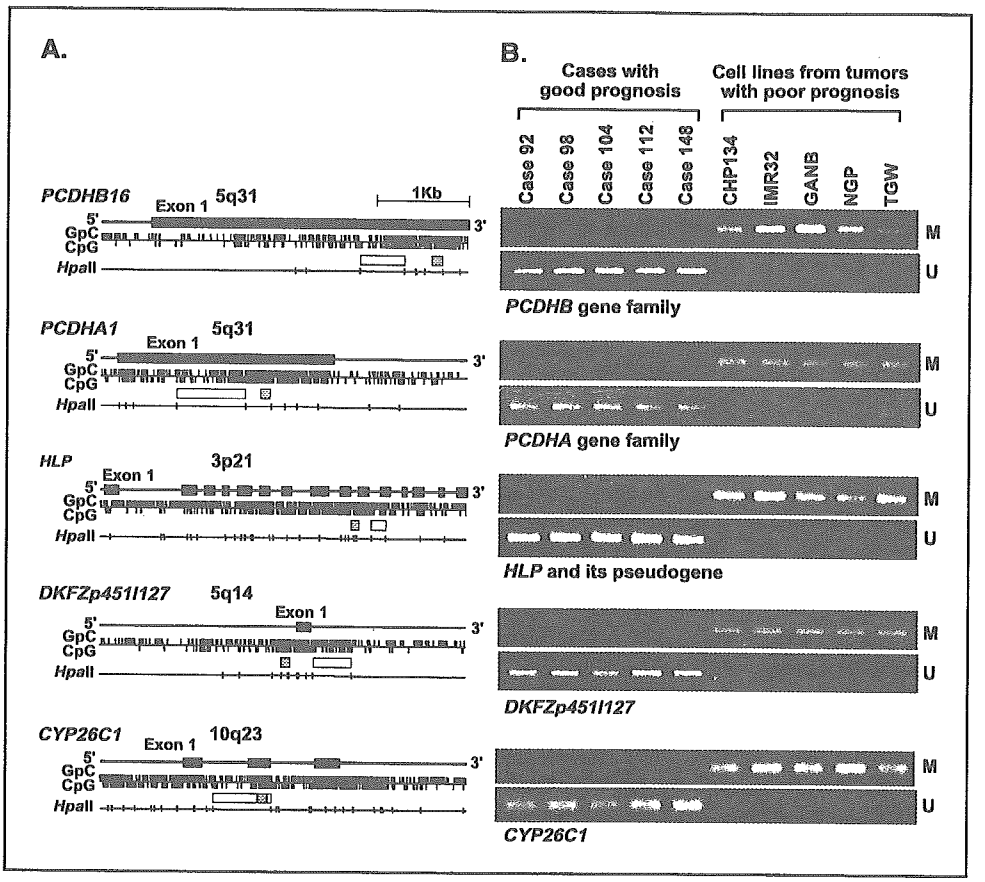

Figure 1. Five CGIs isolated by MS-RDA and their methylation statuses in the samples used for MS-RDA. *A*, genomic structures of the five CGIs. GpC, CpG, and *Hpa*II recognition sites (5′-CCGG-3′) are shown by ticks. *Closed boxes*, exons; *open boxes*, clones isolated by MS-RDA; *shaded boxes*, regions analyzed by MSP. *B*, methylation statuses analyzed by MSP. *M*, MSP using primers specific to methylated DNA; *U*, MSP using primers specific to unmethylated DNA. All the five CGIs were found to be differentially methylated between the two groups used for MS-RDA.

was also done. For each series of MS-RDA, 96 clones were analyzed for redundancy, and nonredundant clones were sequenced. Their genomic origins were examined using BLASTN software http://www.ncbi.nlm.nih.gov/BLAST/).

Sodium Bisulfite Modification and Methylation-Specific PCR. One microgram of DNA underwent sodtlbium bisulfite modification (15), and was suspended in 20 μL of TE buffer. For methylation-specific PCR (MSP), 1 μL of the solution was used for PCR with primers specific to methylated or unmethylated sequences. Using DNA from normal human bronchial epithelial and DNA methylated with *Sss*I methylase, annealing temperatures specific for methylated and unmethylated primers were determined. Quantitative MSP was done separately for methylated DNA molecules and for unmethylated DNA molecules. Standard DNA was prepared by cloning PCR products amplified by methylated and unmethylated primers into a vector, respectively. The numbers of methylated and unmethylated molecules in a test sample were determined by comparing their amplification with those of standard samples containing 10 to 10^6 molecules. The "methylation index" was calculated as the fraction of methylated molecules in the total DNA molecules (no. methylated molecules + no. unmethylated molecules). Each sample was analyzed twice, blind to clinical information, and high reproducibility was confirmed (correlation coefficient = 0.98).

The *protocadherin* β (*PCDHB*) family consists of 16 genes with single exons and three pseudogenes on 5q31, and their CGIs are located in the gene bodies. MSP primers were designed to recognize 17 of the 19 members (all except for the *PCDHB1* gene and the *PCDHB19* pseudogene). The *protocadherin* α (*PCDHA*) family consists of 15 genes and one pseudogene having unique first exons and shared exons 2 to 4 on 5q31, and their CGIs are located in exon 1. MSP primers were designed to recognize 13 of the 16 members (all except for the *PCDHAC1* and *PCDHAC2* genes and the *PCDHA14* pseudogene). The *hepatocyte growth factor-like protein* (*HLP/MSP/MST1*) gene is highly homologous to *macrophage stimulating, pseudogene 9* (*MSTP9*), and MSP primers were designed to recognize both of these. For *DKFZp451I127*, *FLJ37440*, *Zinc finger protein 297* (*ZNF297*), and *Cytochrome p450 CYP26C1* (*CYP26C1*), MSP primers were designed to recognize each of them specifically. The primers and PCR conditions are shown in Supplementary Table 1.

Semiquantitative and Quantitative Reverse Transcription-PCR. cDNA was synthesized from 3 μg of total RNA treated with DNase using a Superscript II kit (Invitrogen Co., Carlsbad, CA). For semiquantitative reverse transcription-PCR (*PCDHB1-PCDHB15*), multiple cycles of PCR were tested for each gene, and numbers giving a wide dynamic range were determined. The primers and PCR conditions are shown in Supplementary Table 2. For quantitative reverse transcription-PCR (*PCDHB16*), the number of cDNA molecules was determined by quantitative PCR, as in quantitative MSP, and the copy number was normalized to that of *GAPDH*.

Chromatin Immunoprecipitation Assay. From 1×10^6 cells, DNA/histone complexes were immunoprecipitated, and DNA was eluted in 30 μL of TE after reversing cross-linking. Copy numbers of DNA molecules of the *PCDHB16* exon, *RASSF1A* promoter, and *GAPDH* promoter in 1 L of the eluate were determined by quantitative PCR (primer sequences in Supplementary Table 3), and normalized to the copy numbers in the input. Anti-acetyl-histone H3 antibody (AcH3) and anti-dimethylated-histone H3 (lysine 9; MetH3K9) were purchased from Cell Signalling (Beverly, MA).

Statistical Analysis. Associations between methylation levels among CGI groups were examined using the Pearson correlation coefficient and Fisher's exact test. Survival time was measured from the date of initial diagnosis to the date of death or last contact. Kaplan-Meier analysis and log-rank tests were done to compare survival between the groups defined by methylation levels. Hazard ratio (HR) between groups and dose-response relationships between methylation levels and survival were estimated by the Cox proportional hazard model. Kaplan-Meier curves were drawn with the help of Aabel software (Gigawiz. Ltd. Co., Tulsa, OK) and other analyses were conducted using SAS version 8.2 (SAS Institute, Inc., Cary, NC).

Results

Genome-Scanning for Differentially Methylated CpG Islands. MS-RDA was done using five primary neuroblastomas with a good prognosis and five neuroblastoma cell lines established from cases with a poor prognosis. Seven DNA fragments, derived from CGIs of *PCDHB16*, *PCDHA1*, *HLP*, *DKFZp451I127*, *FLJ37440*, *ZNF297*, and *CYP26C1*, were isolated as methylated in the latter samples. No DNA fragments were isolated as methylated in the former samples. Methylation statuses of (i) 17 CGIs of the *PCDHB* family (detailed structure in Supplementary Fig. 1), (ii) 13 CGIs of the *PCDHA* family, (iii) *HLP* and its pseudogene, and (iv) other four unique CGIs were examined by MSP. This revealed that the *PCDHB* family (5q31), the *PCDHA* family (5q31), *HLP* (3p21) and its pseudogene (1p36), *DKFZp451I127* (5q14), and *CYP26C1* (10q23) were specifically methylated in the latter samples (Fig. 1*A* and *B*).

Close Association between Methylation and Poor Prognosis in 140 Independent Primary Samples. To analyze the significance of the differential methylation of the above five CGI (groups) in primary neuroblastomas, 140 primary samples, all different from the initial five samples, were analyzed by quantitative MSP. When distributions of methylation indices were analyzed (Fig. 2), a clear bimodal distribution was observed for (i) the CGI group in the *PCDHB* family (17 CGIs), (ii) the CGIs of *HLP* and its pseudogene, and (iii) the *CYP26C1* CGI. The results thus indicated that the cases could be classified into two groups, one with high methylation and the other with low methylation. The dose-response relationships between high *PCDHB* methylation and poor prognosis were analyzed by the Cox proportional model using the methylation index as a continuous value, and the association was confirmed with a trend $P < 0.0001$. Normal adrenal medulla had a methylation index of 4%.

According to the bimodal distribution, the effect of high methylation was assessed by dichotomous groups. For the *PCDHB* family, cutoff values of 30%, 40%, 50%, 60%, 70%, and 80% were tested, and HRs of 16.8 [95% confidence interval (95% CI), 4.0-70.9], 22.1 (95% CI, 5.3-93.4; Fig. 3), 13.1 (95% CI, 4.5-37.9), 9.1 (95% CI, 3.8-23.4), 7.0 (95% CI, 3.1-15.8), and 7.8 (95% CI, 3.4-17.6), respectively, were obtained ($P < 0.001$ for all cutoff values). This showed that cases can be classified into two groups with distinct prognoses, and we adopted a cutoff value of 40%, which gave the highest HR, for convenience in the following analysis.

The dose-response relationships were also confirmed for other four CGI (groups), *PCDHA* ($P = 0.004$), *HLP* ($P < 0.0001$), *DKFZp451I127* ($P = 0.02$), and *CYP26C1* ($P < 0.0001$). Cutoff values were similarly tested, and those for *PCDHA*, *HLP*, *DKFZp451I127*, and *CYP26C1* were set at 80%, 10%, 20%, and 70%, respectively, with HRs of 5.7 (95%CI, 1.4-24.0; $P = 0.07$), 21.7 (95% CI, 5.1-91.4; $P < 0.0001$), 3.2 (95% CI, 1.0-10.5; $P = 0.045$), and 8.7 (95% CI, 4.1-18.1; $P < 0.0001$), respectively (Fig. 3).

Existence of the CpG Island Methylator Phenotype in Neuroblastomas. Methylation of the different CGI (groups) had shown close associations with each other (Table 1). When correlation was analyzed as a continuous value, Pearson correlation coefficients between *PCDHB* and *PCDHA*, *HLP*, *DKFZp451I127* and *CYP26C1* were 0.55, 0.70, 0.26 and 0.77, respectively. This showed that multiple CGIs were simultaneously methylated in

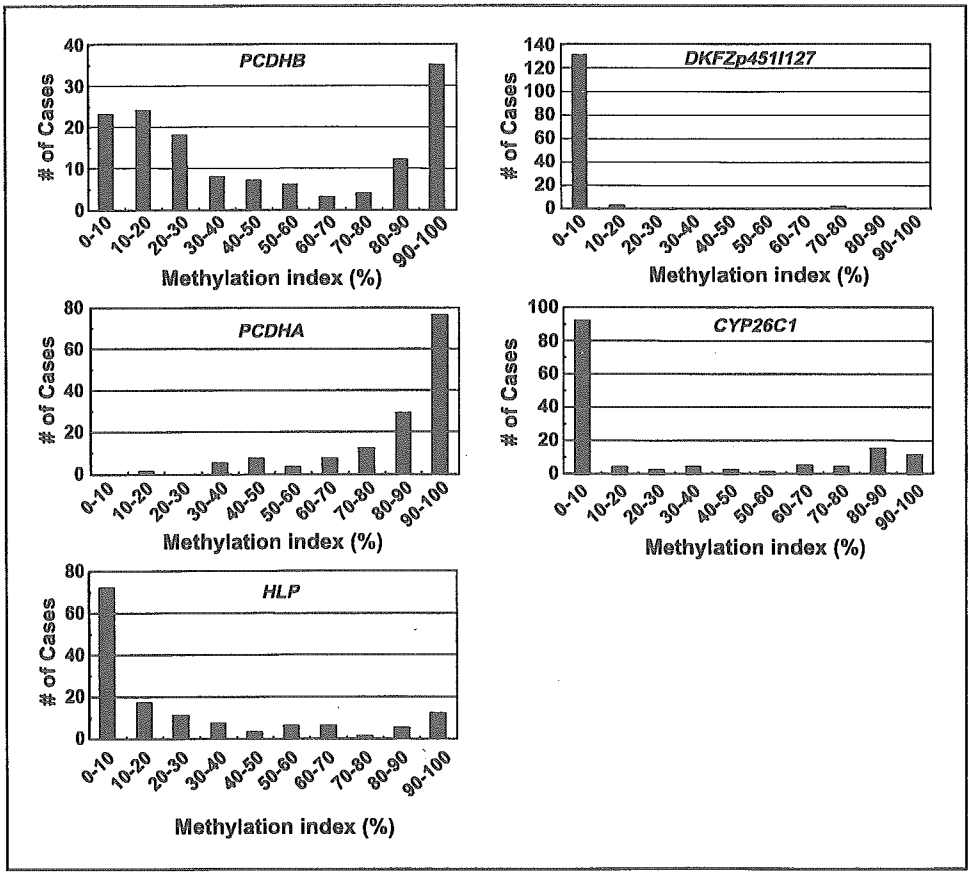

Figure 2. The distribution of methylation indices among the 140 cases analyzed: (*i*) 17 CGIs of the *PCDHB* family, (*ii*) 13 CGIs of the *PCDHA* family, (*iii*) CGIs of *HLP* and its pseudogene, (*iv*) *DKFZp451I127*, and (*v*) *CYP26C1*.

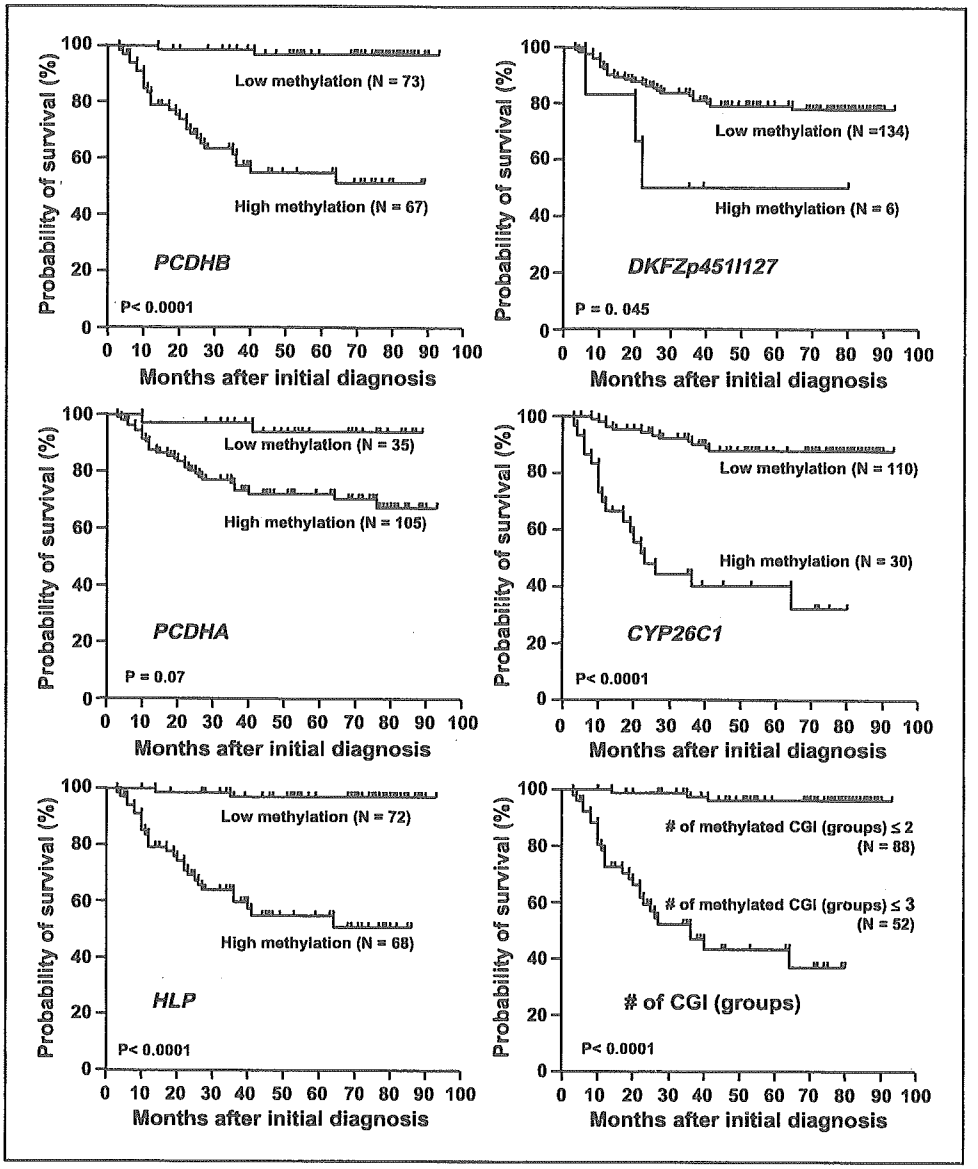

Figure 3. Predictive powers of methylation of the five CGI (groups) identified, and their multiple methylation: (*i*) 17 CGIs of the *PCDHB* family, (*ii*) 13 CGIs of the *PCDHA* family, (*iii*) CGIs of *HLP* and its pseudogene, (*iv*) *DKFZp451I127*, (*v*) *CYP26C1*, and (*vi*) methylation of three of these or more were analyzed by the Kaplan-Meier method using 140 primary samples. The *PCDHB* family, *HLP*, *DKFZp451I127*, *CYP26C1*, and methylation of multiple CGI (groups) had significant influence on survival.

neuroblastomas with a poor prognosis (Supplementary Fig. 2*A*). The simultaneous methylation of (i) 17 CGIs of the *PCDHB* family, (ii) 13 CGIs of the *PCDHA* family, (iii) CGIs of *HLP* and its pseudogene, (iv) *DKFZp451I127* CGI, and (v) *CYP26C1* CGI conformed with the concept of the CpG island methylator phenotype (CIMP; ref. 16).

Associations between CIMP and poor prognosis were examined by defining CIMP as cases with methylation of two CGI (groups) or more, those with three or more, those with four or five, and those with five. When CIMP was defined as cases with methylation of three CGI (groups) or more, the largest association with poor prognosis was observed, with a HR of 25.4 (95% CI, 7.6-84.5; Fig. 3). However, the HR (22.1) given by 17 CGIs of the *PCDHB* gene family approximated to this, and the *PCDHB* methylation level closely correlated with the number of methylated CGI (groups; Supplementary Fig. 2*B*). Therefore, for simplicity of analysis, we defined CIMP in neuroblastomas on the basis of high methylation of the *PCDHB* family, tentatively with a cutoff value of 40%.

Predictive Power of CIMP, Compared with Known Prognostic Factors. Univariate analyses showed that N-*myc* amplification, low *TrkA* expression, DNA diploidy, and an age no younger than 1 year gave HRs of 9.5 (95% CI, 4.4-20.5), 3.9 (95% CI, 1.7-9.3), 4.2 (95% CI, 1.65-10.8), and 12.3 (95% CI, 3.7-41.7). Cases were stratified by these known factors (Table 2). In those without N-*myc* amplification, CIMP also showed an influence with a HR of 12.4 (95% CI, 2.6-58.9), but almost all cases with N-*myc* amplification (37 of the 38 cases) showed CIMP. It was suggested that cases with N-*myc* amplification were contained in the cases with CIMP. CIMP was independent from *TrkA* overexpression, DNA ploidy, and age at diagnosis. Stage seemed to be a stronger prognostic factor. Notably, even when limited to cases in stages III and IV without N-*myc* amplification, which are classified into the intermediate risk group and clinically important, CIMP gave a HR of 4.8 (95% CI, 1.0-23.0; $P = 0.048$).

Multivariate analyses were finally done taking all the five known prognostic factors into account. Although CIMP gave a HR of 5.0 (95% CI, 0.47-52.7), it was not significant ($P = 0.18$), possibly due to limitation in the number of cases.

Table 1. Association between the *PCDHB* methylation and methylation of other CGIs

Variables	Methylation level of *PCDHB* family gene		*P**
	High (≥40%)	Low (<40%)	
No. cases (n = 140)	67	73	
Methylation of CGIs outside promoter regions (n = 140)			
PCDHA gene family (exon 1)†	65/67	41/73	<0.0001
HLP (exons 2-13)‡	52/67	16/73	<0.0001
CYP26C1 (exon 2)§	30/67	0/73	<0.0001
p41Arc (intron 8)	1/67	1/73	0.48
SIM2 (exon 2)	0/67	0/73	
Methylation of CGIs in promoter regions (n = 140)			
DKFZp451I127‖	6/67	0/73	0.011
RASSF1A	51/67	10/73	<0.0001
BLU	25/67	3/73	<0.0001
p16	0/67	0/73	
hMLH1	0/67	0/73	
PCDHB1	0/67	0/73	
TAF7	0/67	0/73	
p41Arc	0/67	0/73	
SIM2	0/67	0/73	

*Fisher's exact test.
†Boundaries for high methylation and low methylation of *PCDHA* gene family were set at 80% of the methylation index.
‡Boundaries for high methylation and low methylation of *HLP* were set at 10% of the methylation index.
§Boundaries for high methylation and low methylation of *CYP26C1* were set at 70% of the methylation index.
‖Boundaries for high methylation and low methylation of *DKFZp451I127* were set at 20% of the methylation index.

Effects of PCDHB Methylation on Gene Expression and Chromatin Structure. The CGIs of the *PCDHB* family were located in their gene bodies, whose methylation generally does not block gene transcription (17). The actual effects of methylation on expression were examined for 16 genes of the *PCDHB* family using 10 primary neuroblastomas with low methylation and five primary neuroblastomas with high methylation. The methylation was not associated with loss of expression (a representative result is shown in Fig. 4*A*). The effect of methylation of the *PCDHB16* CGI on the histone modification was further examined by chromatin immunoprecipitation assay. It was found that DNA methylation of the *PCDHB16* CGI did not induce histone H3 lysine 9 methylation or histone H3 deacetylation (data not shown).

Association between CIMP and Promoter Methylation. High methylation of *PCDHB* CGIs, a sensitive surrogate marker of CIMP in neuroblastomas, did not repress gene expression or induce histone modification. This indicated that CIMP is involved in the poor prognosis of neuroblastomas by causing methylation of promoter CGIs, although it is known that promoter CGIs are resistant to *de novo* methylation (18, 19).

Among the five CGI (groups) identified in this study, only that of *DKFZp451I127* was located in a promoter region. Although its methylation was infrequent, the methylation was observed only in neuroblastomas with CIMP (Table 1), and was associated with expression loss (Fig. 4*B*). To make the association clearer, methylation statuses were analyzed for eight additional CGIs in promoter regions. It was shown that methylation of promoter CGIs of *RASSF1A* (3p21) and *BLU* (3p21) was far more frequently observed in neuroblastomas with CIMP (Table 1, $P < 0.0001$). At the same time, there was a preference for CGIs affected by CIMP among CGIs in promoter regions, and also among those outside promoter regions (Table 2).

Discussion

Extensive methylation of multiple CGIs, conforming with the concept of CIMP, was here found specifically present in neuroblastomas with a poor prognosis and could be sensitively detected by focusing on the *PCDHB* family. *PCDHB* methylation did not suppress gene expression or induce histone modification. However, CIMP was associated with promoter methylation of *RASSF1A* and *BLU* genes and one of the mechanisms underlying the poor prognosis of neuroblastomas seemed to be silencing of these and possibly other tumor suppressor genes and genes important for differentiation.

CIMP was originally identified in colon cancers (16), but there has been some dispute over its presence (20). The clear correlation between CIMP and a poor prognosis found here for neuroblastomas was unequivocal and presumably reflects an intrinsic tendency for methylation of CGIs. This is because, first, neuroblastomas have a much shorter history than colon cancers, and the accumulated number of methylated CGIs in neuroblastomas is expected to parallel the speed of occurrence of

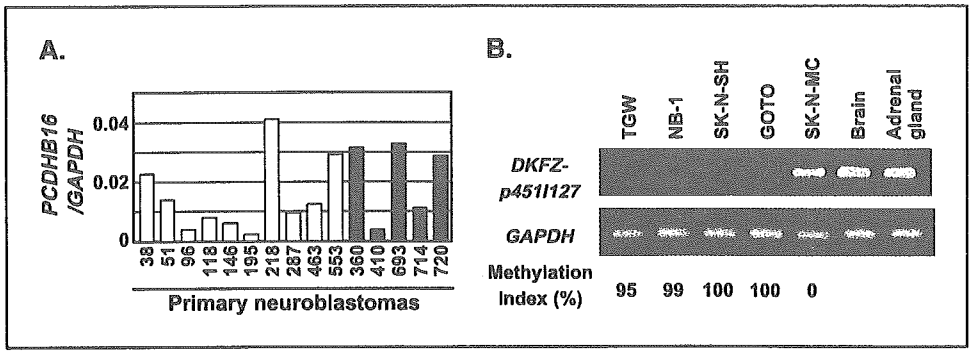

Figure 4. Effects of methylation of the *PCDHB* family and *DKFZp451I127* on gene expression. *A*, *PCDHB16* expression was analyzed by quantitative RT-PCR in 10 primary samples with low methylation (*open columns*) and five primary samples with high methylation (*closed columns*), and no difference was observed between the two groups. *B*, silencing of *DKFZp451I127* by methylation of its promoter CGI. The CGI was methylated in four cell lines, TGW, NB-1, SK-N-SH, and GOTO, whereas it was unmethylated in one cell line, SK-N-MC. *DKFZp451I127* was expressed in SK-N-MC, but not expressed at all in the four cell lines with the promoter methylation.

Table 2. HRs of death by *PCDHB* methylation status in subgroup of known prognostic factors

Stratified by		*PCDHB* methylation	No. cases	No. deaths	HR* (95% CI)	$P^{\dagger}$
Overall (n = 140)		High	67	1	22.1 (5.3-93.4)	< 0.0001
		Low	73	2	1	
N-*myc* amplification (n = 140)	No	High	30	8	12.4 (2.6-58.9)	0.002
		Low	72	2	1	
	Yes	High	37	20	NE	—
		Low	1	0		
TrkA overexpression (n = 130)	Yes	High	20	6	18.3 (2.2-152.6)	0.007
		Low	49	1	1	
	No	High	40	19	NE	
		Low	21	0		
DNA ploidy (n = 125)	Aneuploid	High	17	5	18.3 (2.1-156.7)	0.008
		Low	49	1	1	
	Diploid	High	38	17	NE	
		Low	21	0		
Clinical stages (n = 140)	Stages I, II, and IVS	High	8	0	NE	—
		Low	52	0		
	Stages III and IV	High	59	28	7.4 (1.8-31.3)	0.006
		Low	21	2	1	
Age at diagnosis (n = 140)	<1	High	11	3	NE	
	≥1	Low	59	0		
		High	56	25	4.5 (1.1-18.9)	0.043
		Low	14	2	1	

*HR of death for a case with high *PCDHB* methylation compared with a case with low methylation. NE shows not estimable due to no events in at least one category.
†Significance level for a high *PCDHB* methylation to low methylation using Cox proporitonal model.

methylation. Second, methylation of the *PCDHB* family did not affect gene expression, and there should have been no selection of cells with the *PCDHB* methylation, in contrast to the case of promoter methylation of tumor suppressor genes. Investigation into the mechanism of the intrinsic tendency for methylation of multiple CGIs is necessary. Furthermore, alleviation of the intrinsic tendency could block progression of neuroblastomas and have potential therapeutic value.

Among the six CGI (groups) outside promoter regions analyzed here, CIMP in neuroblastomas preferentially affected four CGI (groups); those of the *PCDHB* family, the *PCDHA* family, *HLP*, and *CYP26C1*. Unexpectedly, three CGIs that are known to be frequently methylated in human colon cancers with CIMP, MINT1, MINT2, and MINT17 (16) were not methylated in neuroblastoma cell lines (data not shown). Among the nine CGIs in promoter regions analyzed, CIMP in neuroblastomas affected only three, those of *RASSF1A*, *BLU*, and *DKFZp451I127*. The nine CGIs were selected based upon previous reports as tumor suppressor genes (*RASSF1A*, *BLU*, *p16*, and *hMLH1*; refs. 21–23), the chromosomal location flanking the *PCDHB* family (*PCDHB1* and *TAF7*), our previous report on the fidelity in inheriting methylation patterns (*p41Arc* and *SIM2*; ref. 19), and the findings here (*DKFZp451I127*). Because gene expression and possibly chromatin structures affect the frequency of *de novo* methylation (24, 25), the available data suggest that CGIs useful to sensitively detect CIMP might vary according to the tumor type.

The influence of CIMP on prognosis was here found to be comparable to that of the currently most reliable marker, N-*myc* amplification, and stronger than *TrkA* overexpression and DNA ploidy on univariate analysis. Subgroup analysis showed that the influence was independent of *TrkA* overexpression, DNA ploidy and age at diagnosis and CIMP had influence even in cases without N-*myc* amplification and in advanced stages. These points strongly indicated CIMP to be a promising new prognostic marker. However, the cutoff values adopted here are tentative, and the HRs obtained could have been overestimated. A validation study using independent samples is necessary for further evaluation. The fact that cases with CIMP contained almost all the cases with N-*myc* amplification suggested that a common molecular mechanism caused both alterations, or that CIMP may lead to N-*myc*

amplification. Whatever the case, the findings might provide clues to molecular mechanisms of neuroblastoma development.

In summary, the present study showed that CIMP is present specifically in neuroblastomas with poor prognosis and that can be sensitively detected by focusing on *PCDHB* methylation. CIMP seems to be a promising new prognostic marker, and its evaluation and investigations into the mechanisms underlying CIMP in neuroblastomas seem warranted.

Acknowledgments

Received 7/27/2004; revised 11/14/2004; accepted 11/24/2004.

Grant support: Grant-in-aid for the Third-term Cancer Control Strategy Program from the Ministry of Health, Labour, and Welfare, Japan and Research Resident Fellowship from the Foundation for Promotion of Cancer Research (M. Abe).

The costs of publication of this article were defrayed in part by the payment of page charges. This article must therefore be hereby marked advertisement in accordance with 18 U.S.C. Section 1734 solely to indicate this fact.

We thank Drs. E. Okochi-Takada and G. S. Goldberg for critical reading of the article and the institutions for participation in the collection of clinical materials.

References

1. Jones PA, Baylin SB. The fundamental role of epigenetic events in cancer. Nat Rev Genet 2002;3:415–28.
2. Chen RZ, Pettersson U, Beard C, Jackson-Grusby L, Jaenisch R. DNA hypomethylation leads to elevated mutation rates. Nature 1998;395:89–93.
3. Kondo Y, Kanai Y, Sakamoto M, et al. Genetic instability and aberrant DNA methylation in chronic hepatitis and cirrhosis-A comprehensive study of loss of heterozygosity and microsatellite instability at 39 loci and DNA hypermethylation on 8 CpG islands in microdissected specimens from patients with hepatocellular carcinoma. Hepatology 2000;32:970–9.
4. Ushijima T, Morimura K, Hosoya Y, et al. Establishment of methylation-sensitive-representational difference analysis and isolation of hypo- and hypermethylated genomic fragments in mouse liver tumors. Proc Natl Acad Sci U S A 1997;94:2284–9.
5. Kaneda A, Takai D, Kaminishi M, Okochi E, Ushijima T. Methylation-sensitive representational difference analysis and its application to cancer research. Ann N Y Acad Sci 2003;983:131–41.
6. Takai D, Yagi Y, Wakazono K, et al. Silencing of *HTR1B* and reduced expression of *EDN1* in human lung cancers, revealed by methylation-sensitive representational difference analysis. Oncogene 2001; 20:7505–13.
7. Kaneda A, Kaminishi M, Yanagihara K, Sugimura T, Ushijima T. Identification of silencing of nine genes in human gastric cancers. Cancer Res 2002;62:6645–50.
8. Miyamoto K, Asada K, Fukutomi T, et al. Methylation-associated silencing of heparan sulfate *D-glucosaminyl 3-O-sulfotransferase-2* (*3-OST-2*) in human breast, colon, lung and pancreatic cancers. Oncogene 2003;22:274–80.
9. Hagihara A, Miyamoto K, Furuta J, et al. Identification of 27 5′ CpG islands aberrantly methylated and 13 genes silenced in human pancreatic cancers. Oncogene 2004;23:8705–10.
10. Brodeur GM. Neuroblastoma: biological insights into a clinical enigma. Nat Rev. Cancer 2003;3:203–16.
11. Schwab M, Westermann F, Hero B, Berthold F. Neuroblastoma: biology and molecular and chromosomal pathology. Lancet Oncol 2003;4:472–80.
12. Nakagawara A, Arima-Nakagawara M, Scavarda NJ, et al. Association between high levels of expression of the *TRK* gene and favorable outcome in human neuroblastoma. N Engl J Med 1993;328:847–54.
13. Jaenisch R, Bird A. Epigenetic regulation of gene expression: how the genome integrates intrinsic and environmental signals. Nat Genet 2003;33:245–54.
14. Li E. Chromatin modification and epigenetic reprogramming in mammalian development. Nat Rev Genet 2002;3:662–73.
15. Kaneda A, Kaminishi M, Sugimura T, Ushijima T. Decreased expression of the seven ARP2/3 complex genes in human gastric cancers. Cancer Lett 2004; 212:203–10.
16. Toyota M, Ahuja N, Ohe-Toyota M, et al. CpG island methylator phenotype in colorectal cancer. Proc Natl Acad Sci U S A 1999;96:8681–6.
17. Gonzalgo ML, Hayashida T, Bender CM, et al. The role of DNA methylation in expression of the *p19/p16* locus in human bladder cancer cell lines. Cancer Res 1998;58:1245–52.
18. Nguyen C, Liang G, Nguyen TT, et al. Susceptibility of nonpromoter CpG islands to *de novo* methylation in normal and neoplastic cells. J Natl Cancer Inst 2001; 93:1465–72.
19. Ushijima T, Watanabe N, Okochi E, et al. Fidelity of the methylation pattern and its variation in the genome. Genome Res 2003;13:868–74.
20. Yamashita K, Dai T, Dai Y, Yamamoto F, Perucho M. Genetics supersedes epigenetics in colon cancer phenotype. Cancer Cell 2003;4:121–31.
21. Agathanggelou A, Dallol A, Zochbauer-Muller S, et al. Epigenetic inactivation of the candidate 3p21.3 suppressor gene *BLU* in human cancers. Oncogene 2003; 22:1580–8.
22. Takita J, Hayashi Y, Nakajima T, et al. The *p16* (*CDKN2A*) gene is involved in the growth of neuroblastoma cells and its expression is associated with prognosis of neuroblastoma patients. Oncogene 1998; 17:3137–43.
23. Harada K, Toyooka S, Maitra A, et al. Aberrant promoter methylation and silencing of the *RASSF1A* gene in pediatric tumors and cell lines. Oncogene 2002; 21:4345–9.
24. De Smet C, Loriot A, Boon T. Promoter-dependent mechanism leading to selective hypomethylation within the 5′ region of gene *MAGE-A1* in tumor cells. Mol Cell Biol 2004;24:4781–90.
25. Richards EJ, Elgin SC. Epigenetic codes for heterochromatin formation and silencing: rounding up the usual suspects. Cell 2002;108:489–500.

Expression profiling using a tumor-specific cDNA microarray predicts the prognosis of intermediate risk neuroblastomas

Miki Ohira,[1,8] Shigeyuki Oba,[2,8] Yohko Nakamura,[1] Eriko Isogai,[1] Setsuko Kaneko,[3] Atsuko Nakagawa,[4] Takahiro Hirata,[5] Hiroyuki Kubo,[5] Takeshi Goto,[5] Saichi Yamada,[6] Yasuko Yoshida,[6] Misa Fuchioka,[7] Shin Ishii,[2] and Akira Nakagawara[1,*]

[1]Division of Biochemistry, Chiba Cancer Center Research Institute, Chiba 260-8717, Japan
[2]Graduate School of Information Science, Nara Institute of Science and Technology, Ikoma 630-0192, Japan
[3]Department of Pediatric Surgery, University of Tsukuba School of Medicine, Tsukuba 305-8575, Japan
[4]Second Department of Pathology, Aichi Medical University, Nagakute 480-1195, Japan
[5]Hisamitsu Pharmaceutical Co. Inc., Tokyo 100-622, Japan
[6]Micro Ceramics Laboratory, R & D Center, NGK Insulators, LTD, Nagoya 467-8530, Japan
[7]Center for Molecular Biology and Cytogenetics SRL Inc., Tokyo 191-0002, Japan
[8]These authors contributed equally to this work.
*Correspondence: akiranak@chiba-cc.jp

Summary

To predict the prognosis of neuroblastoma patients and choose a better therapeutic protocol, we developed a cDNA microarray carrying 5340 genes obtained from primary neuroblastomas and examined 136 tumor samples. We made a probabilistic output statistical classifier that provided a high accuracy in prognosis prediction (89% at 5 years) and a highly reliable method to validate it. Kaplan-Meier analysis indicated that the patients in an intermediate group defined by existing markers are divided by microarray into two further groups with 5 year survivals for 36% and 89% of patients ($p < 10^{-4}$), i.e., with unfavorably and favorably predicted neuroblastomas, respectively. According to these results, we developed a gene subset chip for a clinical tool, for which our classifier exhibited 88% prediction accuracy.

Introduction

Neuroblastoma is one of the most common solid tumors in children and originates from the sympathoadrenal lineage of the neural crest (Bolande, 1974). Its clinical behaviors are heterogeneous. The tumor, when developed in infants, frequently regresses spontaneously by inducing differentiation and/or programmed cell death. When developed in children over 1 year of age, however, the tumor is often aggressive and acquires resistance to intensive chemotherapy. Although recent progress in therapeutic strategies against advanced neuroblastoma has improved patient survival, long-term outcomes still remain very poor. Furthermore, part of neuroblastomas categorized to the intermediate group (stage 3 or 4 tumors that possess a single copy of the *MYCN* gene) often recurs after complete response to initial therapy. Such differences in the final outcomes of the tumor are considered presumably attributable to differences in genetic and biological abnormalities, which are reflected in the gene and protein expression profiles of the tumor.

The prediction of cancer prognosis is one of the most urgent demands to initiate the treatment of neuroblastoma. As expected from the natural course of neuroblastoma, patient age at diagnosis (over or under 1 year of age) is an important prognostic factor (Evans et al., 1971). Disease stage is also a powerful indicator for neuroblastoma prognosis (Brodeur et al., 1993). Moreover, recent advances in basic research have discovered several molecular markers that are useful in clinical practice, including amplification of the *MYCN* oncogene (Schwab et al., 1983; Brodeur et al., 1984), DNA ploidy (Look et al., 1984; Look et al., 1991), deletion of chromosome 1p (Brodeur et al., 1988), and *TrkA* expression (Nakagawara et al., 1992; Nakagawara et al., 1993). Other indicators also include *telomerase* (Hiyama et al., 1995), *CD44* (Favrot et al., 1993), *pleiotrophin* (Nakagawara et al., 1995), *N-cadherin* (Shimono et al., 2000), *CDC10* (Nagata et al., 2000), and *Fyn* (Berwanger et al., 2002). However, the combinations thereof still frequently fail to predict patient outcome. In the post-genome sequence era, therefore, the advent of new diagnostic tools has been ex-

SIGNIFICANCE

Neuroblastoma is an enigmatic tumor with heterogeneous clinical behaviors including maturation, regression, and growth. Despite recent improvements in the cure rate of many pediatric tumors, the prognosis of advanced neuroblastoma is still poor. In addition, it is usually difficult to predict the prognosis of the intermediate risk group in advanced stages without *MYCN* amplification. Through our supervised machine learning and highly reliable statistical validation procedure with the 5 year prognosis of the patients, we established a simple, low-cost microarray system carrying top-ranked genes, which exhibited high accuracy (88%) to predict the neuroblastoma prognosis and is highly feasible as a clinical tool.

pected. Recently, the DNA microarray method, applied to comprehensively demonstrate expression profiles of primary neuroblastomas and cell lines, has already identified the following: (1) differences in gene expression between favorable and unfavorable subsets (Yamanaka et al., 2002; Berwanger et al., 2002); and (2) differences in gene expression that occur during retinoic acid-induced neuronal differentiation (Ueda, 2001). However, a study to predict neuroblastoma prognosis with a microarray using a large number of neuroblastoma samples has never been reported. We have recently isolated 5500 genes from the cDNA libraries, which were generated from primary neuroblastomas, part of which has previously been reported (Ohira et al., 2003a; Ohira et al., 2003b). In this study, to identify genes strongly associated with neuroblastoma prognosis and to apply them to make a really practical cDNA microarray for neuroblastoma diagnosis, we constructed an in-house, ink-jet-printed cDNA microarray carrying 5340 genes proper to neuroblastoma and applied it to analyze 136 samples. After selecting genes significantly related to patient prognosis, we made a mini-chip carrying 200 top-ranked genes to apply for the clinic.

There have been many attempts to predict cancer outcome using microarray. A reliable prediction for outcomes of cancer patients naturally demands its reproducibility, and it is quite important to use sound and highly reliable statistical methodologies; a complete crossvalidation analysis without introducing any information leakage and an independent test using new samples are necessary. As Ntzani and Ioannidis (2003) pointed out, however, such a careful methodology has often been ignored in most microarray studies. We here developed a supervised classification method without any information leakage as a statistic tool and demonstrated that the probabilistic output of the analysis defines the molecular signature of neuroblastoma to predict its prognosis. Although the construction of the statistical tool was based on one of the most reliable statistical tests, we also consulted a validation test for an independent experiment examining 50 samples (whose RNAs were prepared in an independent laboratory) by using the mini-chip. The high performance for the outcome prediction by the mini-chip system suggests the high feasibility of developing a clinical tool based on molecular signature.

Results

Neuroblastoma proper cDNA microarray

The whole scheme of our study is summarized in Figure 1. We first constructed a neuroblastoma proper cDNA microarray harboring the spots of 5340 genes on a slide glass by using a ceramics-based ink-jet printing system (the 5340 genes system). This in-house cDNA microarray appeared to have overcome the previous problems caused by pin-spotting, e.g., uneven quantity or shape of individual spots on an array. Ten micrograms each of the total RNA extracted from 136 frozen tissues of primary neuroblastomas were labeled with Cy3 dye. As a common reference, the mixture of the total RNA obtained from four neuroblastoma cell lines with a single copy of *MYCN* (NB69, NBLS, SK-N-AS, and SH-SY5Y) was labeled with Cy5 dye.

We first evaluated the quality of our cDNA microarray, the 5340 genes system. The log Cy3/Cy5 fluorescence ratio of each gene spot was normalized to eliminate intensity-dependent biases. Since the 5340 genes array contains 260 duplicated or multiplicated genes, the expression ratio of such a duplicated gene was represented by the average of multiple spots. Based on estimation performance for missing values (see the Supplemental Data available with this article online) and on reproduction variance of the duplicated genes, the standard deviation for the log ratio of a single gene was sufficiently small, ranging between about 0.2 and about 0.3 (Figure S1A). The scatter plots of the log Cy3/Cy5 fluorescence ratio between duplicated gene spots in the 136 experiments and those between repeated experiments also indicated high reproducibility of spotting and experiment (Figures S1B and S1C). These suggest that the production of and experiments by our cDNA microarray are highly reproducible.

Supervised classification

To develop a statistical tool that predicts the prognosis of a new patient with neuroblastoma, we introduced a supervised classification. In the development, we used 136 neuroblastomas, randomly selected tumor samples from the neuroblastoma tissue bank, consisting of 41 stage 1 tumors, 22 stage 2 tumors, 33 stage 3 tumors, 28 stage 4 tumors, and 12 stage 4s tumors. The follow-up duration ranged between 3 and 241 months (median, 56 months, mean, 57.3 months) after diagnosis. The left panel in Figure 2 compiles summary information of each sample, including survival time and important prognosis markers (see Experimental Procedures for details). Since variations in follow-up duration generated noises in the supervised classification, we used patient outcome (dead or alive) at 5 years after diagnosis as the target label to be predicted. Since the outcomes of 40 of 136 samples were unknown at 5 years after diagnosis, data for 96 remaining samples were used subsequently. When we were interested in short-term outcome prediction, the target label was set at 2 years after diagnosis, for which purpose 126 samples out of the 136 samples were used.

We constructed the weighted voting as a supervised classifier after important genes were selected according to pairwise *F* scores. To estimate the prediction accuracy for new data, we consulted leave two out (LTO) analysis, which obtains almost unbiased estimation of prediction accuracy for new data while avoiding overestimation due to information leakage (Figure S2A). Although it is known that the prediction accuracy of a supervised classifier depends on the number of genes to be used (Figure S3), the LTO procedure enables us to optimize it without introducing information leakage, by using a sample left out at the outer loop of the double-loop procedure (see Experimental Procedures). The crossvalidation accuracy for the 5 year prognosis prediction was as high as 88.5% (sensitivity of 86.7% and specificity of 89.4%) (Table 1, "Whole cases"). In the LTO analysis, we selected genes and constructed the corresponding classifier individually for the outcome prediction of each sample. The average number of the selected genes, n, was 30.7. If we applied the same procedure to the short-term (2 year) prediction, the accuracy, sensitivity, and specificity were 89.8%, 88.0%, and 90.2%, respectively (data not shown).

Construction of a probabilistic output

According to the LTO analysis, we can obtain weighted vote values and the corresponding survival rates. After approximat-